# AN ADDITIVE TURBULENT DECOMPOSITION OF THE NAVIER-STOKES EQUATIONS IMPLEMENTED ON HIGHLY PARALLEL COMPUTER SYSTEMS

**(Final Report)**



J. M. McDonough
E. C. Hylin
Y. Yang
X. Zhong

*Department of Mechanical Engineering*
*University of Kentucky*

Tony F. C. Chan
T. Matthew

*Mathematics Department*
*University of California, Los Angeles*

UNCLASSIFIED

# REPORT DOCUMENTATION PAGE

Form Approved
OMB No 0704-0188



| 1. AGENCY USE ONLY (Leave blank) | 2. REPORT DATE | 3. REPORT TYPE AND DATES COVERED |
|---|---|---|
| | 5 August 1991 | FINAL |

**4. TITLE AND SUBTITLE**
An Additive Turbulent Decomposition of the Navier Stokes Equations Implemented on Highly Parallel Computer Systems

**5. FUNDING NUMBERS**
G AFOSR 90-0271
PE 61102F
PR 2707
TA A1

**6. AUTHOR(S)**
McDonough, J.M., Hylin, E.C., Chan, Tony F.C. and Matthew, T. , Y. Yang, X. Zhong

**7. PERFORMING ORGANIZATION NAME(S) AND ADDRESS(ES)**
University of Kentucky
Dept. of Mechanical Engr.
Lexington, KY 40506-0046

Subcontract:
University of California
405 Hilgard Avenue
Los Angeles, CA 90024

**8. PERFORMING ORGANIZATION REPORT NUMBER**
N/A

**9. SPONSORING/MONITORING AGENCY NAME(S) AND ADDRESS(ES)**
AFOSR
Building 410
Bolling AFB
Washington, DC 20332-6448

**10. SPONSORING/MONITORING AGENCY REPORT NUMBER**
AFOSR 90-0271

**11. SUPPLEMENTARY NOTES**
N/A

**12a. DISTRIBUTION/AVAILABILITY STATEMENT**
Approved for Public Release;
Distribution Unlimited

**12b. DISTRIBUTION CODE**

**13. ABSTRACT** (Maximum 200 words)

Progress is reported on a study of a new turbulence simulation technique based on unaveraged, additive decomposition of the Navier-Stokes equations. The decomposition formalism provides a natural separation of the governing equations into large- and small-scale parts, with the small scale solved in local subdomains. The method thus exhibits a high degree of automatic parallelism, and in addition is well-suited for application of domain decomposition methods as part of the solution process. Results presented include validation of a 2-D version of the small-scale equations, initial studies associated with bifurcation of solutions to these equations, qualitative comparisons with data, and analysis of the additive turbulent decomposition in 2-D, generalized coordinates.

| 14. SUBJECT TERMS | 15. NUMBER OF PAGES |
|---|---|
| Turbulence Simulation, Navier-Stokes Equations, Additive Decomposition, Large Eddy Simulation, Transition | 15 |
| | 16. PRICE CODE |

| 17. SECURITY CLASSIFICATION OF REPORT | 18. SECURITY CLASSIFICATION OF THIS PAGE | 19. SECURITY CLASSIFICATION OF ABSTRACT | 20. LIMITATION OF ABSTRACT |
|---|---|---|---|
| Unclassified | Unclassified | Unclassified | UL |

# 1. INTRODUCTION

This report documents work performed on AFOSR Grant 90-0271 — "An Additive Turbulent Decomposition of the Navier-Stokes Equations Implemented on Highly Parallel Computer Systems." The work was performed at the University of Kentucky (UK), and (on a subcontract to the grant) at UCLA, during the period 1 June 1990 to 31 May 1991. A report on the first four months of effort was submitted in the form of an Annual Report at the end of October, 1990. We shall begin this report by presenting some background information, following this with a brief summary of the first four months of work and then the main body of the report. The main items treated in this report will represent work completed during the period 1 October 1990 to 31 May 1991; they include our continuing work on the transition to turbulence in channel flow, the beginnings of a 2-D implementation of the additive turbulent decomposition (ATD) in generalized coordinates, work on the interaction between chemical kinetics and turbulence, and further analyses of ATD and domain decomposition. We shall end with a summary of our work on this project as a whole, including all work supported by AFOSR grants 90-0271 and 89-0281, and will list the publications and presentations which have resulted from this work.

## 1.1 Background

Additive turbulent decomposition (ATD) is an approach to turbulence simulation, first proposed by McDonough, et al. [1], who were motivated by the observation that none of the present methods for turbulence simulation are really acceptable for the broad range of turbulent flows that must be analyzed for practical engineering problems. The classical methods — mixing length, k-ε, and Reynolds stress models — are efficient enough, but are not predictive. Moreover, if the Reynolds averaging procedure on which these methods are based corresponds to time averaging, the results will not even be consistent with the Navier-Stokes equations. On the other hand, higher-level techniques such as large eddy simulation (LES) and direct numerical simulation (DNS) provide results that are generally consistent with solutions to the Navier-Stokes equations, and are predictive or nearly so, but they are not efficient enough for application to high Reynolds-number (Re) engineering problems on present or forseeable computing hardware.

In a structural sense, ATD lies in between LES and DNS. Large-scale and small-scale components of a flow field are treated separately, corresponding respectively to the resolved and subgrid-scale (SGS) parts of LES, but (unlike LES) no formal averaging or filtering is employed in constructing the equations of ATD. In particular, the governing equations are split into large- and small-scale parts by an additive decomposition. There are cross-terms connecting these equations but, in contrast to LES, there are equations for each separate factor in these cross-terms, so there is no closure problem. An additional advantage of ATD is that the algorithm lends itself to a high level of parallelization. Thus, on computers with many parallel processors, the clock time required to perform a simulation can be greatly reduced. Section 2.2 below describes a parallel ATD algorithm.

In the process of splitting the governing equations into equations for the large- and small-scale parts of a flow, ATD requires the introduction of decomposition parameters. These may be selected arbitrarily, but one selection at least has a clear physical interpretation. This is the particular decomposition identified by Hylin in McDonough, et al.[2], in which the split equations for the velocity time-derivatives are in the form of *transport* equations for the large- and small-scale momentum. For incompressible flow these equations are:

$$\frac{\partial \mathbf{u}}{\partial t} + \nabla\cdot(\mathbf{uu}) + \nabla\cdot(\mathbf{u}^*\mathbf{u}) = -\nabla p + \frac{1}{\mathrm{Re}}\Delta\mathbf{u} \qquad (1\text{-}1)$$

$$\frac{\partial \mathbf{u}^*}{\partial t} + \nabla\cdot(\mathbf{u}\mathbf{u}^*) + \nabla\cdot(\mathbf{u}^*\mathbf{u}^*) = -\nabla p^* + \frac{1}{Re}\Delta \mathbf{u}^* \tag{1-2}$$

$$\nabla\cdot\mathbf{u} = \delta \tag{1-3}$$

$$\nabla\cdot\mathbf{u}^* = -\delta \tag{1-4}$$

where $\delta$ is a decomposition divergence, which we set equal to zero. These equations form the basis for the work below, except for the 1-D work on chemical kinetics and turbulence, and the work described in the appendix.

### 1.2 Summary of the Work Performed from June through September, 1990.

During the first four months of the current grant, we completed the initial development of a numerical algorithm for solving the small-scale Navier-Stokes equations in a 2-D cell. As a test problem, we imposed periodic boundary conditions on the cell and looked at the evolution of a vortical perturbation under the influence of a uniform large-scale shear. The preliminary results demonstrated that the algorithm was accurate to at least second-order in time, and that the flow seemed to be related to other flows describable in terms of "inner coordinates."

Another part of our work in the first four months was concerned with analyses of the 2-D implementation of ATD in generalized coordinates. The goal of this work is to gain an understanding of what is required in order to construct reasonably portable ATD modules that can be added to existing CFD codes to enhance their turbulence simulation capabilities. We chose to employ a Fourier-Galerkin representation of the small-scale equations and looked at the issue of including metric information in the Galerkin inner products. We also began the development of a code for the large-scale Navier-Stokes equations, employing generalized coordinates in two dimensions. The code is based on a projection method like that employed by Kim and Moin [3], extended to generalized coordinates and using intermediate boundary conditions that result in second-order temporal accuracy. The individual split steps are quasi-linearized in $\delta$-form and solved via Douglas-Gunn time-splitting [4].

Lastly, we continued to examine the mathematical relations between ATD and related methods, including the development of fast solvers for elliptic problems using domain decomposition techniques.

## 2. TRANSITION TO TURBULENCE IN CHANNEL FLOW

### 2.1 Implementation of the Small-Scale Equations

*2.1.1 Summary of Work to Date.* In our most recent report [5], we mentioned our implementation of the 2-D small-scale equations. This uses a Chebyshev tau method for the spatial discretization of the equations, the Crank-Nicolson method for the temporal discretization of the linear velocity terms, and a second-order predictor-corrector method for the temporal discretization of the nonlinear and pressure gradient terms. The resulting equations are in Helmholtz or Poisson form, and we solve them by means of a variation on the Haidvogel-Zang algorithm [6,7].

We first implemented the small-scale equations using periodic boundary conditions on the velocity but, as discussed below, these later proved unsuitable for our test problem. Furthermore, a full implementation of the ATD algorithm requires a combination of Dirichlet and Neumann conditions on the boundaries of the small-scale cells. Accordingly, we have modified our computer code for the small-scale equations to handle an arbitrary combination

of Dirichlet and Neumann conditions. The code supports up to 33 Chebyshev modes in each direction, and can use for the velocity any initial condition which meets the mode restriction and is zero on the boundaries. With minor modifications, the small-scale code is ready to be used as a subroutine in an implementation of the complete ATD algorithm for 2-D flow in rectangular geometries.

*2.1.2 Description of the Test Problem.* As a test problem, we have examined the decay of a vortical perturbation in a single small-scale cell, subject to a uniform large-scale shear. We initially imposed periodic boundary conditions [5], but imposition of the proper pressure boundary condition — that identified by Gresho and Sani [8] — showed that the small-scale pressure was *not* periodic, and hence that periodic boundary conditions were not appropriate. The symmetry inherent in the definition of the test problem, together with the results obtained using periodic boundary conditions, then led us to examine rotationally symmetric boundary conditions of order two. Interestingly, imposing these proved to be identical to imposing homogeneous Dirichlet conditions on all four boundaries, i.e., to using a completely closed boundary, which is also inappropriate for this flow.

This identity, however, led to a test of a projection technique which will be used in an implementation of the full ATD algorithm to ensure that the small-scale solution is globally continuous. Briefly, this technique uses Lagrange multipliers to project onto a divergence-free subspace a trial solution for the velocity fluxes through the boundaries. We used this technique in conjunction with the condition on rotational symmetry, and compared the resulting solution to that obtained by imposing homogeneous Dirichlet conditions directly. The two solutions were identical almost to machine precision, completely validating the projection technique.

The appropriate boundary conditions for this flow turn out to be those corresponding to an isolated vortex — one far from any boundaries to the large-scale flow — or a "semi-isolated" vortex — one bounded by a wall on one side only. For the isolated vortex, open (i.e., flow-through) boundary conditions are used on all four sides of the cell, while for the semi-isolated vortex, open conditions are used on three sides and a homogeneous Dirichlet condition is used on the side representing the wall. We are currently modeling open boundaries by imposing an homogeneous Neumann condition on the velocities, and on all boundaries have used a homogeneous Neumann condition for the pressure. This latter condition, especially, is not quite correct [8], but a recent paper by Gresho suggests that the errors may be confined close to the boundaries [9].

The small-scale test problem is defined in a square, $x \in [-1,1]$, $y \in [-1,1]$, and the initial small-scale perturbation is given by the stream function:

$$\psi = C\,(\,1 - 4x^2 + 6x^4 - 4x^6 + x^8\,)\,(\,1 - 4y^2 + 6y^4 - 4y^6 + y^8\,) \qquad (2\text{-}1)$$

where $C$ is a constant expressing the *strength* of the perturbation. This stream function yields a vortex which has zero velocity on the boundary of the defining square. In fact, the velocity is $C^2$ on the boundary. The perturbation pressure is determined by using the perturbation velocity in the Poisson equation for the small-scale pressure:

$$\Delta p^* = \nabla\cdot\left(\frac{1}{Re}\Delta \mathbf{u}^* - \nabla\cdot(\mathbf{u}\mathbf{u}^*) - \nabla\cdot(\mathbf{u}^*\mathbf{u}^*)\right) \qquad (2\text{-}2)$$

On solid boundaries we used for the perturbation pressure the Neumann condition identified by Gresho and Sani [8]; with the given stream function, this becomes an *homogeneous* Neumann condition. On open boundaries we set the perturbation pressure to zero, which implicitly sets the initial acceleration on those boundaries. Setting the initial pressure on open boundaries to zero also ensures that the pressure is $C^0$ on the boundary. Thus defined,

both the velocity perturbation and the pressure perturbation have compact support.

The form of the initial vortex is given by equation 2-1. If, additionally, the initial strength is held constant, then the test problem is governed by a single parameter, which may be expressed either as a Reynolds number or as a non-dimensional vortex diameter. The two are related according to

$$\lambda^+ \equiv \lambda \sqrt{\frac{du/dy}{\nu}} = 2\sqrt{Re} \tag{2-3}$$

where $\lambda$ is the diameter of the initial vortex, du/dy is the shear strain-rate for the large-scale flow, and Re is the half-diameter Reynolds number.

*2.1.3 Results to Date for the Test Problem.* We have solved the problem described above for Reynolds numbers ranging from 1 to 3000. For the cases we have simulated, figures 2-1 and 2-2 show the decay or growth of the Chebyshev-weighted $L^2$ norm of the small-scale velocity field:

$$\|\mathbf{u}^*\|_{L^2_w} \equiv \left\{ \int_{-1}^{1} \int_{-1}^{1} \mathbf{u}^* \cdot \mathbf{u}^* \frac{dx}{\sqrt{1-x^2}} \frac{dy}{\sqrt{1-y^2}} \right\}^{\frac{1}{2}} \tag{2-4}$$

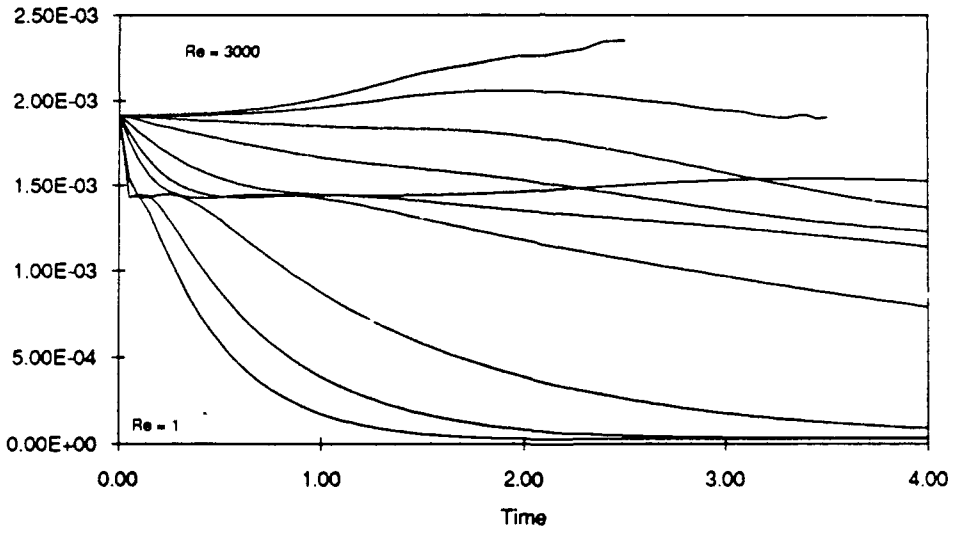


Figure 2-1. Decay of the velocity norm of an isolated vortex.

In most of the cases shown, there is an initial transient — due to our particular initial and boundary conditions — followed by a long period of decay. The rate of decay becomes slower and more unsteady as the Reynolds number is increased, and at high enough Reynolds numbers the vortex grows in strength. Similar behavior is shown in figure 2-3, which focuses on the growth or decay of the (0,1) component of the small-scale x-velocity. This component is constant in the x-direction, and linear in the y-direction, and for low Reynolds numbers is a mode which decays slowly. For Reynolds numbers below 10, the decay of the

(0.1) mode is evident in the figure. For Reynoids numbers from 10 to 300, the initial transient lasts longer than the time frame shown in the figure, but we believe that the corresponding curves do eventually decay. For Reynolds numbers of 1000 and 3000, however, an initial decay is followed by the appearance of an oscillation which grows in amplitude. Thus, figure 2-3 suggests a transition Reynolds number somewhere in the range of 300 to 1000. We should mention here that the time-step size for these simulations was $10^{-4}$, so the period of the oscillations is many times the time-step size and thus the oscillations are not due to a numerical instability.

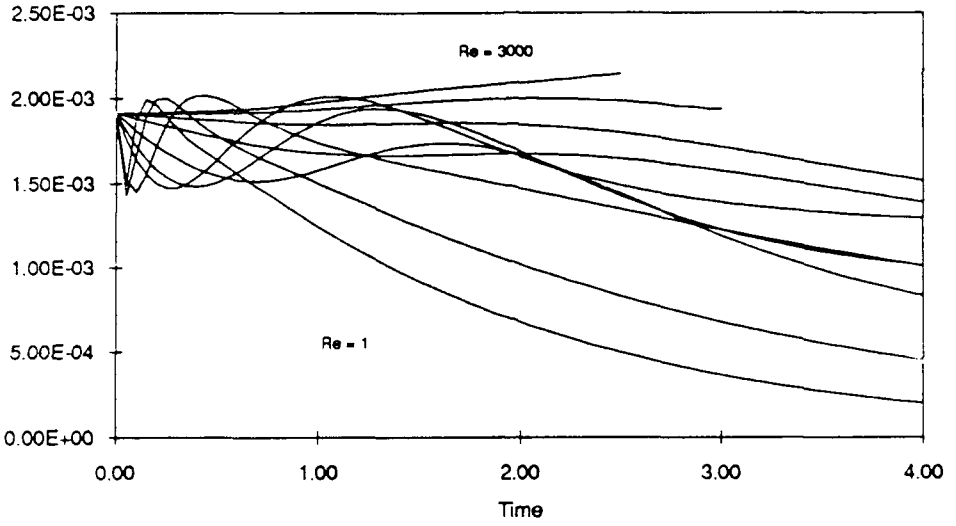


Figure 2-2. Decay of the velocity norm of a semi-isolated vortex.

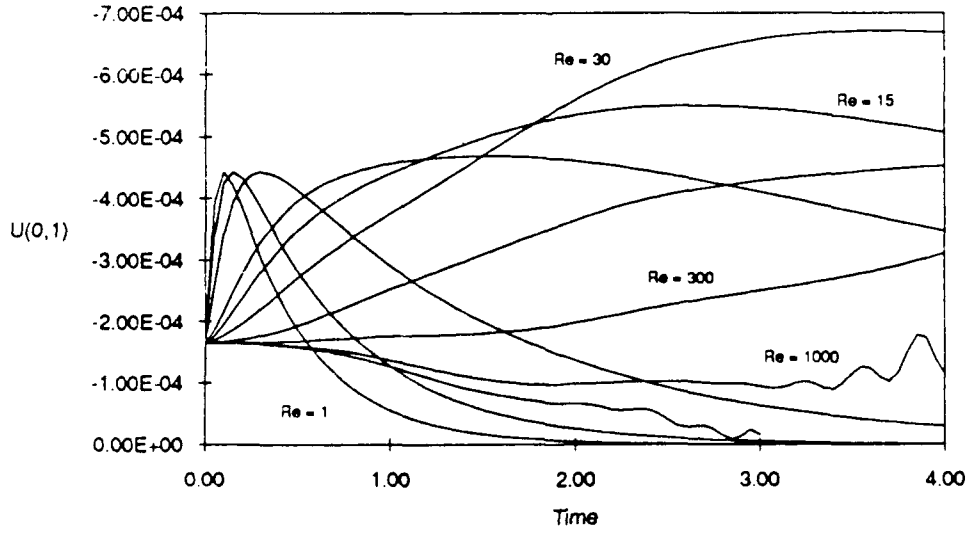


Figure 2-3. Decay of the (0,1) mode of the x-velocity for an isolated vortex.

Recall that the Reynolds number in this problem is related by equation 2-3 to a non-dimensional diameter $\lambda^+$. In figure 2-4, the initial and late-stage decay rates of the velocity norm for an isolated vortex are plotted as functions of $\lambda^+$. A late-stage curve for the semi-isolated vortex was not plotted because some of the curves in figure 2-2 do not seem to have settled down to an asymptotic decay rate by the end of the simulation, but the early-stage curves for the semi-isolated and isolated vortices are identical. The values of $\lambda^+$ which are of special interest are those where the curves cross the zero line and the $-1$ line. Vortical disturbances smaller than the former value tend to be damped out, while larger disturbances are amplified and may begin to affect the large-scale flow. The two curves in figure 2-4 cross the $-1$ line at $\lambda^+ = 3$ and $\lambda^+ = 8$, and the late curve seems to cross the zero line for some $\lambda^+$ between 10 and 70. Vortical disturbances with $\lambda^+$ smaller than 3 to 8 are damped so rapidly that they have a negligible effect on the overall flow; they decay in less time than it takes the fluid nearby to travel a distance comparable to the vortex diameter. Vortical disturbances with $\lambda^+$ larger than a transition value between 10 and 70 begin to grow in strength. The results in figure 2-3 suggest that the transition value lies between $\lambda^+ = 35$ (Re=300) and $\lambda^+ = 63$ (Re=1000). These values are consistent with our previous results, even though the boundary conditions are different.

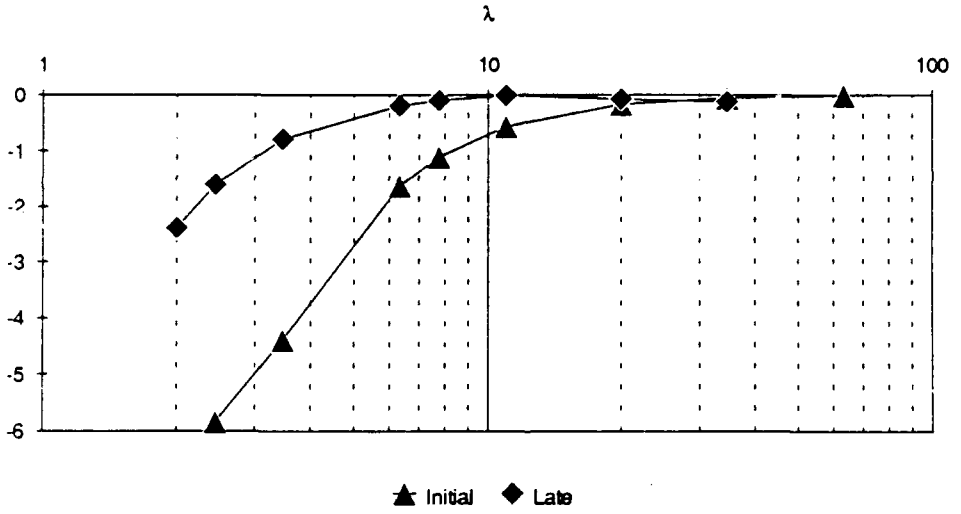


Figure 2-4. Growth rate of the velocity norm vs. $\lambda^+$

As described in our most recent report [5], $\lambda^+$ is expressed in "inner coordinates." The same values of $\lambda^+$ declared above to be significant are also significant in the environment for which inner coordinates were originally defined: the inner layers of a wall-bounded turbulent flow. In such a situation, $\lambda^+ < 5$ corresponds to the laminar sublayer, $5 < \lambda^+ < 70$ corresponds to the transition region, and $\lambda^+ > 70$ corresponds to the fully turbulent outer flow. The close correspondence between these values and the results we have obtained show that the latter are consistent with and provide a possible explanation for a well-known body of experimental data.

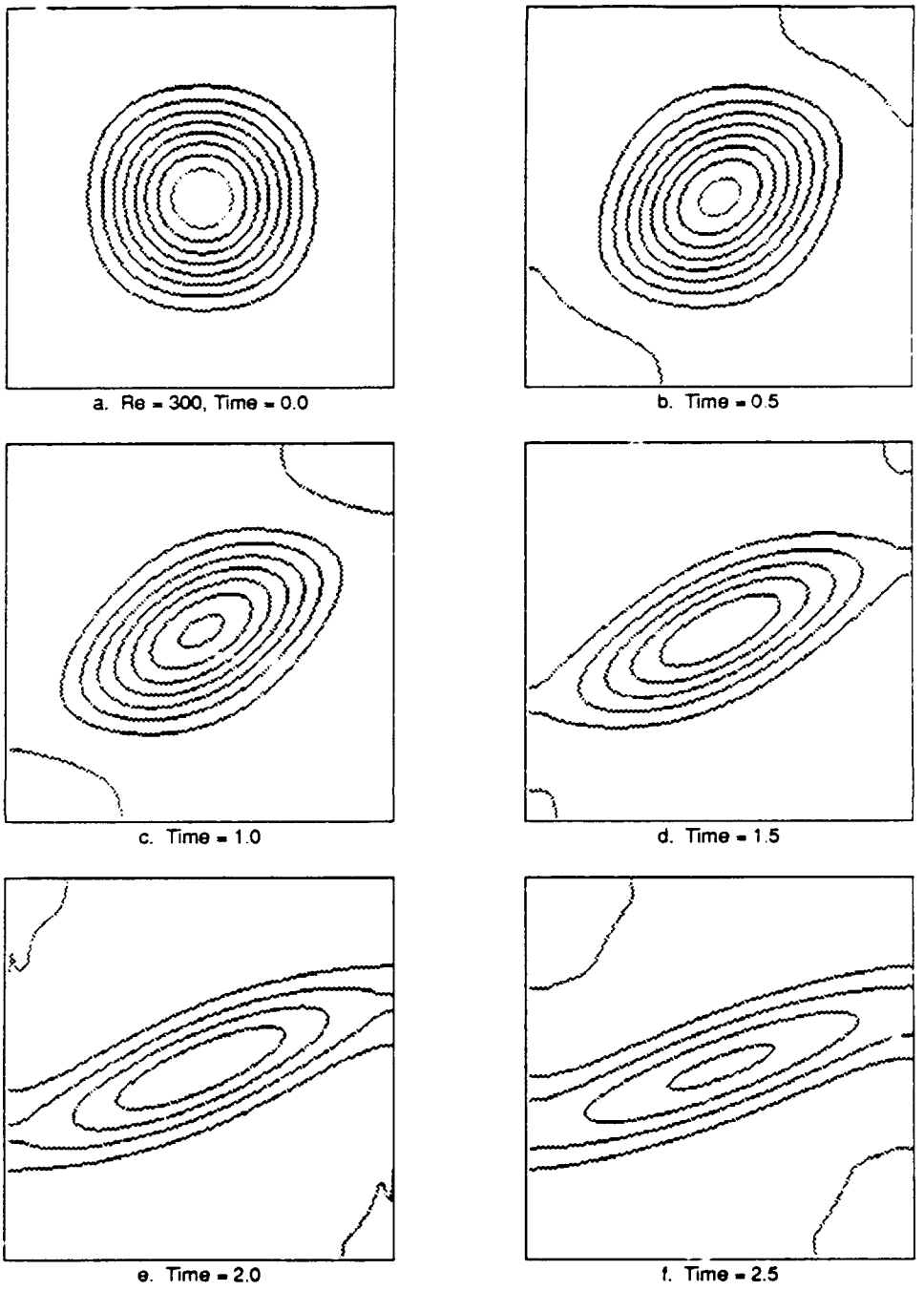


Figure 2-5. Evolution of stream function contours for an isolated vortex.

The structural evolution of the vortex is affected both by the large-scale shear and by the influence of the Reynolds number (or the non-dimensional vortex diameter). Figure 2-5 shows the evolution of the stream function contours for an isolated vortex at a Reynolds number of 300. The shear flow moves to the right at the top of the cell and to the left at the bottom, and the vortex is rotating counter-clockwise. As might be expected, the large-scale

shear causes a tilting and elongation of the vortex, but it also tends to cause an intensification of the vorticity, an effect which becomes apparent at high Reynolds numbers. This is illustrated in figure 2-6, which shows the vorticity contours for three cases: Re = 100 ($\lambda^+ = 20$), Re = 300 ($\lambda^+ = 35$), and Re = 1000 ($\lambda^+ = 63$), as well as for the initial condition. When Re = 100, the vorticity gradually decays, but when Re = 300 or above, the vorticity becomes more intense with time. This suggests that transition for this flow may begin in the neighborhood of Re = 300.

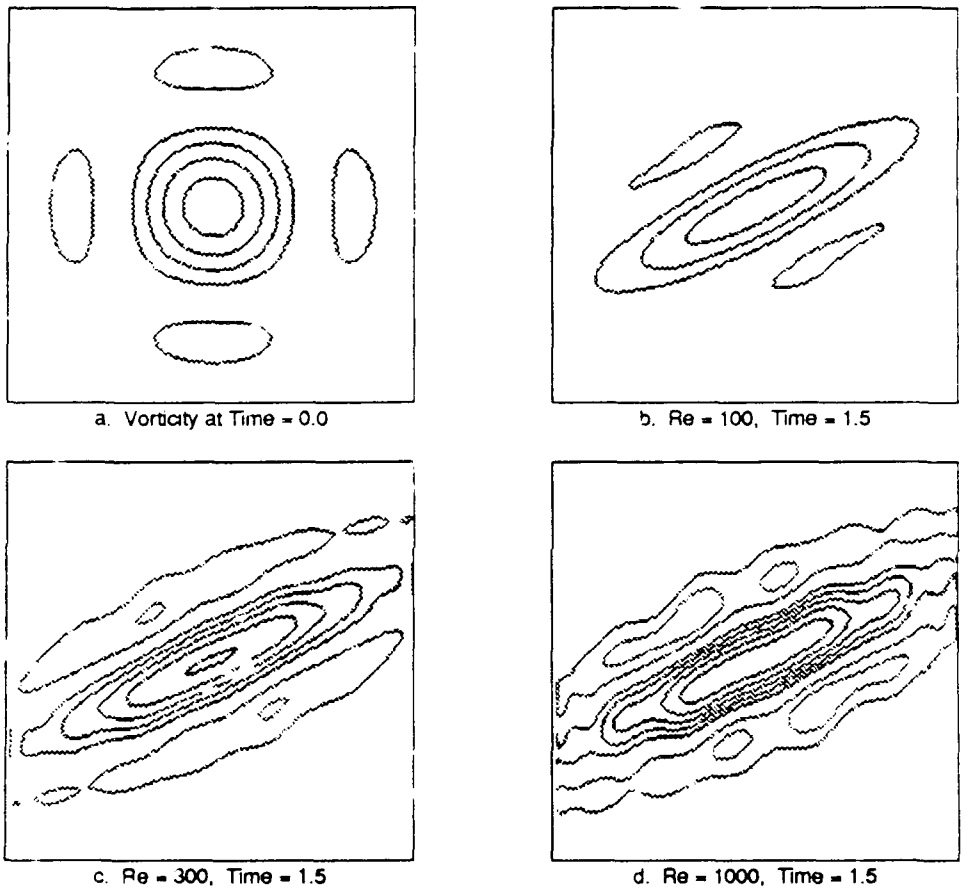


Figure 2-6. Intensification of vorticity at high Reynolds numbers.

The structural evolution of a semi-isolated vortex is qualitatively similar to the evolution of an isolated vortex, but — in the case when the vortex is rotating counter-clockwise — the presence of the wall induces negative vorticity and positive flow between the vortex and the wall. This is evident in figure 2-7, where the wall is on the bottom side of each square. The decay of a semi-isolated vortex is prolonged by the presence of a virtual vortex on the other side of the wall but, as shown by a comparison of figures 2-1 and 2-2, the presence of the wall also causes qualitative changes in the decay transient. At present, the reasons for these changes are not known.

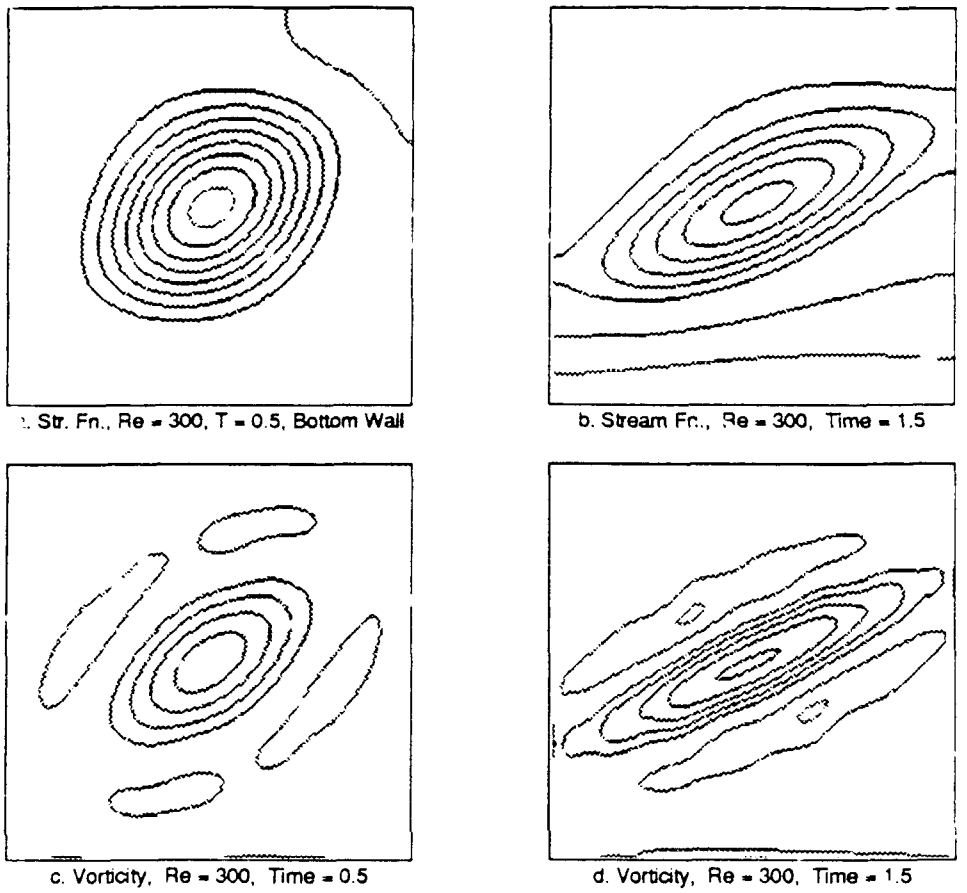


Figure 2-7. Evolution of a semi-isolated vortex.

While figures 2-1 through 2-3 and figure 2-6 show results for $Re = 1000$ and $Re = 3000$, and while the early results for these cases look acceptable, we were unable to carry the integrations for these cases beyond a certain point without the computations blowing up. In these cases, however, we have observed that the vortex appeared to be stretched beyond the confines of the simulation cell. It may be that as the vortex starts to grow, it begins to exert a significant influence on the flow beyond the cell boundaries, which is not included in our model. This should not be a problem in the complete ATD algorithm (except possibly at outflow boundaries), because the neighboring cells will then be present and flow between cells will be accounted for. At outflow boundaries the boundary conditions will have to be treated carefully; certainly more carefully than we have treated them in this test problem.

## 2.2 Definition of a Complete, Parallelizable ATD Algorithm

We have continued to proceed with the implementation of the complete ATD procedure for the Navier-Stokes equations, applied to the case of 2-D channel flow, and have identified an algorithm which in some circumstances can be completely parallelized. This algorithm incorporates and makes extensive use of the previously described algorithm for the 2-D small-scale equations [5]. In the text below, we shall first present the algorithm and then discuss each step in detail. In the listing of the algorithm, each level of indentation indicates

either a loop structure or parallelization at the subroutine level.

*Algorithm*

*Predict the large-scale solution at the next large-scale time step.*
*For each small-scale cell:*
    *Project the large-scale solution onto the small-scale basis.*
*For each small-scale time step:*
    *For each small-scale cell:*
        *Interpolate the large-scale solution for the current time.*
        *Carry out the preliminary small-scale solution.*
    *While not converged:*
        *For each cell interface:*
            *Smooth the velocities across the interface.*
        *Project the smoothed velocities onto a divergence-free subspace.*
        *For each cell:*
            *Re-solve the small-scale problem.*
*For each small-scale cell:*
    *Restrict the solution onto the large-scale basis.*
*Correct the large-scale solution at the new large-scale time.*

*2.2.1 Predict the large-scale solution at the next large-scale time step.* This is the first step in the ATD solution algorithm defined by McDonough [2,10]. Supposing that the over-all algorithm is to be $p^{th}$ order accurate, and that n large-scale time steps have been completed. In this step of the current algorithm, we calculate a $p-1^{th}$ order prediction of the large-scale solution at the $n+1^{th}$ step. We will probably implement this step serially, using the same solution routine we have developed for the small-scale equations. However, as long as the time-discretization is carried out such that the resulting semi-discrete equations are in Poisson or Helmholtz form, the many techniques which have been developed for the parallel solution of Poisson's equation may be used to construct a parallelized procedure for this step in the algorithm. Assuming that we use the serial routine that we have on hand, if there are N small-scale cells in an approximately square array, and one large-scale data point per cell, this step will require approximately $O(N^{3/2})$operations.

*2.2.2 ..Project the large-scale solution onto the small-scale basis.* After transmission of the large-scale solution to each processor, this step can be carried out in parallel on as many processors as there are small scale cells. If there are M small-scale data points in each cell ($M^{1/2}$) modes in each direction, this step will take $O(N \times (M^{1/2}N + MN^{1/2} + M \log M))$ operations.

*2.2.3 For each small-scale time step...* The small-scale time step is typically much smaller than the large-scale time step. This statement in the algorithm begins a loop which runs until the solution for the small-scale flow has evolved from the $n^{th}$ large-scale time step to the $n+1^{th}$.

*2.2.4 Interpolate the large-scale solution for the current time.* The statement: *"For each small-scale cell:"* begins a section of code which is parallelizable. The first step in this section is to interpolate the large-scale solution for the current small-scale time. Recall that the large-scale solution has been estimated to $p-1^{th}$ order accuracy at the $n+1^{th}$ large-scale

time. In order for the small-scale solution to be accurate, and because the small-scale time step is much smaller than the large-scale time step, interpolation of the large-scale solution between the values at the $n^{th}$ and $n+1^{th}$ times is required. If $p = 2$, a linear interpolation will suffice, in which case this step requires $O(M)$ operations per cell, or $O(NM)$ operations altogether.

*2.2.5 Carry out the preliminary small-scale solution.* Once the large-scale solution has been interpolated to the current small-scale time, a preliminary solution of the small-scale equations is carried out in each cell. This may be done in parallel if there is more than one processor. Using our small-scale solution routine, this step requires $O(M^{3/2})$ operations per cell, or $O(NM^{3/2})$ operations altogether. The results are only *preliminary* because we do not yet have sufficient information to accurately update the velocities on the cell *boundaries*. Getting this information requires iteration.

*2.2.6 While not converged...* This statement begins a loop in which the velocities on the cell boundaries are updated and the solution to the small-scale equations is recalculated. This is repeated until the solution converges. The convergence criterion is a function of the large-scale and small-scale time steps, as well as of the accuracy required on the large scale.

*2.2.7 Smooth the velocities across the interface.* In any solution of an elliptic problem which is carried out by means of a domain decomposition, it is necessary to smooth the solution across the boundaries of the subdomains. This may be accomplished by various methods, several of which we have already examined in connection with ATD [10,11,12]. Here we propose to fit a fifth-order polynomial across each boundary, matching the small-scale velocity solutions with $C^2$ continuity at the nearest Chebyshev collocation point on either side. Evaluating the polynomial at the boundary will then provide an updated value for the boundary velocity.

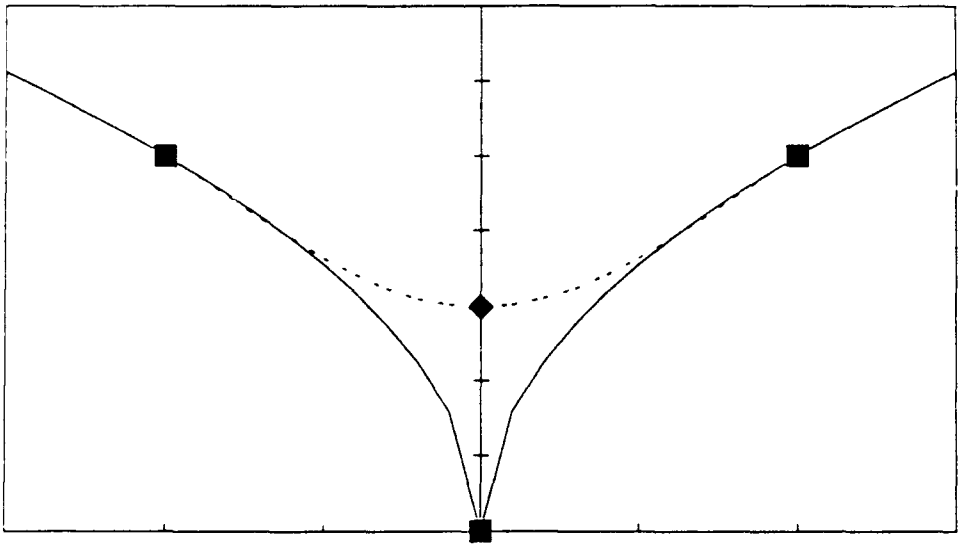

Figure 2-8. Smoothing of the small-scale velocity profile.

This technique is shown schematically in figure 2-8, where the solid lines represent the unsmoothed solution and the dashed lines represent the polynomial. Because the fitted

polynomial blends smoothly with the old velocity profiles, the new boundary value for the velocity at this stage satisfies the small-scale momentum equations to at least $O(h)$, where h is the distance from the boundary to the nearest collocation point. This step in the algorithm requires $O(M \log M)$ operations per cell, or $O(NM \log M)$ operations altogether. It may be parallelized, in which case communication is required between the processors holding data for adjacent cells.

*2.2.8 Project the smoothed velocities onto a divergence-free subspace.* This is a crucial step, and was alluded to in section 2.1. The smoothed velocities on the cell boundaries do not necessarily satisfy the requirement for mass conservation. In this step, the mass flux across each cell boundary is first computed using the new boundary velocities. Then, Lagrange multipliers are employed to adjust the *fluxes* until they satisfy the zero-divergence (mass conservation) constraint, while changing the fluxes as little as possible. The constraints on this optimization problem do not change — they are determined by geometry alone — but the data (the cell divergences) are different each time the problem is solved. The problem can be reduced to a set of matrix/vector multiplications, requiring $O(N^2)$ operations, and there are many existing algorithms which may be used to parallelize this step.

*2.2.9 For each cell, re-solve the small-scale problem.* In each cell, the small-scale equations are solved once again, using the updated values for the velocities on the boundaries. Note that only the boundary values for the small-scale *velocities* are updated. The boundary condition for the pressure is always determined in *each* cell from the momentum equation applied on the boundary (c.f. Gresho and Sani [8]). As before, this step requires $O(M^{3/2})$ operations per cell, or $O(NM^{3/2})$ operations altogether.

*2.2.10 Restrict the solution onto the large-scale basis.* Once the small-scale solution has been advanced to the $n+1^{th}$ large-scale time step, it is necessary to restrict the small-scale solution onto the large-scale basis, so that the large-scale solution may be corrected. This requires $O(NM)$ operations altogether, and the restriction may be carried out in all cells in parallel.

*2.2.11 Correct the large-scale solution at the new large-scale time.* This is the *last* step in the ATD solution algorithm identified by McDonough, and corrects the previous large-scale solution to $p^{th}$ order at the new time. Once again, if we use the same code we have been using to solve the small-scale equations, this step will require approximately $O(N^{3/2})$operations.

*2.2.12 Summary of operation counts.* If we take K time steps on the small scale for each time step we take on the large scale, and if L iterations are required at each small-scale step for the solution to converge, then one step through the above algorithm requires

$$O(M^{1/2}N^2 + MN^{3/2} + MN \log M + KM^{3/2}N + KLM^{3/2}N + KLN^2 + KLMN \log M)$$

operations. Because the algorithm is completely parallelizable, many of these operations can be carried out simultateously if more than one processor is available. Minimizing execution clock-time, however, will depend on minimizing the amount of communication required between processors, as well as the operation count of each parallelized step. This will impel careful consideration of how the data are distributed to the various processors.

## 3. ATD FOR 2-D INCOMPRESSIBLE FLOW IN GENERALIZED COORDINATES

Our current work on ATD in generalized coordinates is divided into two parts: first, implementation of the large-scale equations using a chaotic map to simulate the effects due to the small scale; and second, implementation of the small-scale equations with an imposed large-scale flow. Not until both implementations have been checked out and understood will they be combined to form a complete ATD procedure.

### 3.1 The Large-Scale Equations in Generalized Coordinates

The code that we are developing to solve the large-scale incompressible Navier-Stokes equations in 2-D generalized coordinates is based on a projection method. In such a method, the Navier-Stokes momentum equations are solved with the pressure-gradient term omitted, and the solution is then *projected* onto a divergence-free velocity field. The resulting solution satisfies the continuity equation exactly, while the momentum equation is satisfied only approximately, but the error in the momentum equation can be kept small enough for the method to be of practical use.

The derivation of the large-scale equations in generalized coordinates is complex and is here omitted, as are the equations themselves. Details are in Appendix A. As is generally the case in ATD, there are cross-terms in the large-scale equations which involve the small-scale velocities. Initially, instead of obtaining the small-scale velocities by solving the small-scale equations, we will model them by means of a chaotic map which we will develop, with the expectation that the large-scale equations derived via ATD and used in conjunction with such a map may be able to simulate more general turbulent flows than is possible with LES and the current models for subgrid-scale effects.

So far we have derived the generalized-coordinate versions of the large-scale momentum equations without the pressure gradient terms. These equations have been implemented in VS FORTRAN on the *IBM 3090-600J supercomputer at UK, and constitute* the first step in the projection algorithm. Our next tasks in this area are to implement the projection step, and to develop the chaotic map to model the small-scale velocities.

### 3.2 The Small-Scale Equations in Generalized Coordinates

We have decided to use a Fourier-Galerkin procedure for the solution of the small-scale equations in generalized coordinates, in part because we believe that it will be applicable for a wide range of problems, and in part because it is easier to implement in the context of generalized coordinates than is the Chebyshev-tau approach used in the channel flow problem. In particular, it is possible to arrange things such that the basis functions satisfy the small-scale continuity equation (1-4) mode by mode. This requires the introduction of the contravarient velocities U and V:

$$U = \xi_x u + \xi_y v \qquad V = \eta_x u + \eta_y v \,, \tag{3-1}$$

where $\xi_x$ , $\eta_y$ , etc. are elements of the Jacobian matrix of the coordinate transformation. Then the small-scale continuity equation in generalized coordinates becomes

$$\left(\frac{U^{\bullet}}{J}\right)_{\xi} + \left(\frac{V^{\bullet}}{J}\right)_{\eta} = 0 \,, \tag{3-2}$$

which has a structure very similar to that in the Cartesian coordinates. Here $J = \xi_x \eta_y - \xi_y \eta_x$ .

To construct the local approximation, we consider a cell centered at $(\xi_i , \eta_i)$ and

assume that the solution can be represented by truncated Fourier series, defined as follows,

$$U^*(\xi,\eta,t) = J\sum_{k,l}^{K} a(t)_{kl}\cos\alpha_k \frac{\xi-\bar{\xi}_i}{h}\sin\alpha_l \frac{\eta-\bar{\eta}_i}{h} \tag{3-3a}$$

$$V^*(\xi,\eta,t) = J\sum_{k,l}^{K} b_{kl}(t)\sin\alpha_k \frac{\xi-\bar{\xi}_i}{h}\cos\alpha_l \frac{\eta-\bar{\eta}_i}{h} \tag{3-3b}$$

$$p^*(\xi,\eta,t) = \sum_{k,l}^{K} c_{kl}(t)\sin\alpha_k \frac{\xi-\bar{\xi}_i}{h}\sin\alpha_l \frac{\eta-\bar{\eta}_i}{h} \tag{3-3c}$$

where

$$\bar{\xi}_i = \xi_i - \frac{h}{2}, \quad \bar{\eta}_i = \eta_i - \frac{h}{2},$$

$$\alpha_k = k\pi, \qquad \alpha_l = l\pi,$$

and h is the finite difference grid spacing for the large-scale calculation. A major advantage of in choosing the basis functions as defined by equation 3-3 is that when we construct Galerkin inner products we can eliminate the Fourier coefficient for pressure in a way similar to that suggested by Orszag and Kruskal [13] (See also Canuto, et. al, [7]).

$$c_{kl} = \frac{k\, f_{kl} + l\, g_{kl}}{k\, \xi_x + l\, \eta_y}. \tag{3-4}$$

where $f_{kl}$ and $g_{kl}$ are the Galerkin inner products of the nonlinear terms. (See Appendix A).

Using the basis functions defined in equation 3-3, we have derived the Fourier-Galerkin representation of the small-scale equations in generalized coordinates. The derivation of the small-scale momentum equations in generalized coordinates is complex and is here omitted, as are the equations themselves — details are in Appendix A — but the derivation gives a set of ODE's for the coefficients $\dot{a}_{kl}$ and $\dot{b}_{kl}$. We solve this system of ODE's via a second-order explicit Runge-Kutta method (Heun's method). We will be using the code based on these equations to investigate the convergence of Fourier-Galerkin approximations to chaotic solutions of the Navier-Stokes equations, and to investigate the effects of bifurcation parameters such as the Reynolds number and the local gradients of the large-scale velocity on the nature of solutions to the small-scale Navier-Stokes equations.

## 4. CHEMICAL KINETICS/TURBULENCE INTERACTION

It is extremely difficult to simulate the details of interactions between turbulence and other physical phenomena. Reynolds-averaged approaches, and LES, employ modeling on precisely the length and time scales where interactions are likely to be important, and DNS is too expensive to be able to produce the desired results for complex engineering problems. During the past year we have begun to study the use of the small-scale equations of ATD as local parametrized (with large-scale properties) DNS. We have completed an initial simulation corresponding to the tip of an $H_2$-$O_2$ diffusion flame at low Mach number (–

0.05), and moderate Re (~ 6000). Details of these studies are reported by McDonough and Saito [14].

Here, we begin by presenting the governing equations being used, in dimensionless form, the 1-D, (nearly) compressible, viscous Navier-Stokes and species equations:

$$\rho_t + (\rho u)_x = 0 \tag{4-1a}$$

$$(\rho u)_t + (\rho u^2)_x - \frac{1}{Re}\, u_{xx} = -p_x \tag{4-1b}$$

$$T_t + (uT)_x - \frac{1}{Pe_T}\, T_{xx} = \frac{A\hat{T}^2}{\rho c_p}(\rho Y_1)^2 (\rho Y_2)\, e^{-E/\mathcal{R}^0\tilde{T}} \tag{4-1c}$$

$$(\rho Y_i)_t + (\rho u Y_i)_x - \frac{1}{Pe_D}\,(\rho Y_{i,x})_x = -C_i\hat{T}^2(\rho Y_1)^2 (\rho Y_2)\, e^{-E/\mathcal{R}^0\tilde{T}}, \qquad i = 1, 2. \tag{4-1d,e}$$

In these equations

$$Re \equiv \frac{\rho^0 U^0 L}{\mu^0}, \quad Pe_T \equiv \frac{U^0 L}{\alpha^0}, \quad Pe_D \equiv \frac{U^0 L}{D^0}, \tag{4-2}$$

where $Pe_T$ and $Pe_D$ are, respectively, thermal and mass diffusion Peclét numbers;

$$A \equiv \frac{L\rho^{0^2} T^0 B}{c_p^0 U^0}\left(\frac{2h_1^0}{W_1 W_2} + \frac{h_2^0}{W_1^2}\right), \tag{4-3}$$

and

$$C_1 \equiv \frac{2L\left(\rho^0 T_{ref}\right)^2 B}{U^0 W_1 W_2}, \qquad C_2 \equiv \frac{L\left(\rho^0 T_{ref}\right)^2 B}{U^0 W_1^2}. \tag{4-4}$$

$T_{ref}$ is a reference temperature (different from $T^0$), and B is the pre-exponential factor. $\tilde{T}$ is the dimensional, unshifted temperature, and $\hat{T}$ is the corresponding dimensionless quantity.

We apply the additive turbulent decomposition in the manner described by McDonough and Saito [14], and then using the Fourier representation

$$\rho^*(x,t) = \sum_{k=1}^{K} a_k(t)\sin\sigma_{kh}x^*, \tag{4-5a}$$

$$m^*(x,t) = \sum_{k=1}^{K} b_k(t)\cos\sigma_{kh}x^*, \tag{4-5b}$$

$$T^*(x,t) = \sum_{k=1}^{K} c_k(t)\sin\sigma_{kh}x^* , \tag{4-5c}$$

$$z_1^*(x,t) = \sum_{k=1}^{K} d_k(t)\sin\sigma_{kh}x^* , \tag{4-5d}$$

$$z_2^*(x,t) = \sum_{k=1}^{K} e_k(t)\sin\sigma_{kh}x^* , \tag{4-5e}$$

where $\sigma_{kh} = k\pi/h$, and $x^* \equiv x-(x_i-h/2)$, with $x\in[x_i-h/2, x_i+h/2]$, we construct a local Galerkin procedure which leads to the small-scale ODE's

$$\dot{a}_k = \sigma_{kh} b_k \tag{4-6a}$$

$$\dot{b}_k = \sum_{i,j=1}^{K}\left[\frac{\pi}{\rho}jB_{ijk}+\frac{\rho_x}{2\rho^2}hC_{ijk}\right]b_i b_j - \frac{1}{Re}\left[\frac{1}{\rho}\sigma_{kh}^2+\frac{1}{\rho^3}\left(\rho\rho_x-2\rho_x^2\right)+\frac{\overline{m}_x}{\rho}-\frac{\rho_x\overline{m}}{\rho^2}\right]b_k$$
$$-\frac{D}{2}\left[\pi\sum_{i,j=1}^{K}(jD_{ijk}+iD_{jik})\left(\frac{d_j}{W_1}+\frac{e_j}{W_2}\right)c_i+\overline{T}_x\left(\frac{d_k}{W_1}+\frac{e_k}{W_2}\right)+\left(\frac{\overline{z}_{1,x}}{W_1}+\frac{\overline{z}_{2,x}}{W_2}\right)c_k\right] \tag{4-6b}$$

$$\dot{c}_k = \sum_{i,j=1}^{K}\left[\frac{\pi}{2\rho}(iA_{ijk}-jB_{kij})-\frac{\rho_x}{2\rho^2}hD_{jik}\right]b_i c_j - \frac{1}{Pe_T}\left[\sigma_{kh}^2+\frac{1}{2}\left(\frac{\rho_x}{\rho^2}+\frac{\overline{m}_x}{\rho}\right)\right]c_k + \frac{\pi}{4\rho}b_k + \frac{A}{\rho c_p}f_k \tag{4-6c}$$

$$\dot{d}_k = \frac{\pi}{2\rho}\sum_{i,j=1}^{K}(iA_{ijk}-jB_{kij})b_i d_j - \frac{1}{Pe_D}\left(\sigma_{kh}^2-\frac{\overline{m}_x}{\rho}+\frac{\rho_{xx}}{\rho}-1\right)d_k - C_1 f_k \tag{4-6d}$$

$$\dot{e}_k = \frac{\pi}{2\rho}\sum_{i,j=1}^{K}(iA_{ijk}-jB_{kij})b_i e_j - \frac{1}{Pe_D}\left(\sigma_{kh}^2-\frac{\overline{m}_x}{\rho}+\frac{\rho_{xx}}{\rho}-1\right)e_k - C_2 f_k , \tag{4-6e}$$

$$k = 2, 3, \ldots, K ,$$

where

$$f_k \equiv \left\{\overline{z}_1^2\overline{z}_2\hat{T}c_k + \frac{h}{2}\left[\sum_{i,j=1}^{K}\left(\overline{z}_1^2\overline{z}_2 c_i+2\overline{z}_1\overline{z}_2\hat{T}d_i+\overline{z}_1^2\hat{T}e_i\right)c_j A_{ijk}\right.\right.$$
$$\left.\left.+\sum_{i,j,l=1}^{K}\left(2\overline{z}_1\overline{z}_2 d_i c_j+\overline{z}_1^2 e_i c_j+\overline{z}_2\hat{T}d_i d_j+2\overline{z}_1\hat{T}d_i e_j\right)c_l E_{ijlk}\right] \tag{4-7}$$

$$+\sum_{i,j,l,m=1}^{K}(\bar{z}_2 d_i c_j + 2\bar{z}_1 e_i c_j + \hat{T} d_i e_j) d_l c_m F_{ijlmk}$$
$$+\sum_{i,j,l,m,n=1}^{K} d_m d_n e_i c_j c_l G_{ijlmnk}\Bigg]\Bigg\} e^{-E/\mathcal{R}^0\bar{T}},$$

with

$$A_{ijk} \equiv \int_{x_i-\frac{h}{2}}^{x_i+\frac{h}{2}} \sin\sigma_{ih}x^* \sin\sigma_{jh}x^* \sin\sigma_{kh}x^*\, dx \tag{4-8a}$$

$$B_{ijk} \equiv \int_{x_i-\frac{h}{2}}^{x_i+\frac{h}{2}} \cos\sigma_{ih}x^* \sin\sigma_{jh}x^* \cos\sigma_{kh}x^*\, dx \tag{4-8b}$$

$$C_{ijk} \equiv \int_{x_i-\frac{h}{2}}^{x_i+\frac{h}{2}} \cos\sigma_{ih}x^* \cos\sigma_{jh}x^* \cos\sigma_{kh}x^*\, dx \tag{4-8c}$$

$$D_{ijk} \equiv \int_{x_i-\frac{h}{2}}^{x_i+\frac{h}{2}} \sin\sigma_{ih}x^* \cos\sigma_{jh}x^* \sin\sigma_{kh}x^*\, dx \tag{4-8d}$$

$$E_{ijlk} \equiv \int_{x_i-\frac{h}{2}}^{x_i+\frac{h}{2}} \sin\sigma_{ih}x^* \sin\sigma_{jh}x^* \sin\sigma_{lh}x^* \sin\sigma_{kh}x^*\, dx \tag{4-8e}$$

$$F_{ijlmk} \equiv \int_{x_i-\frac{h}{2}}^{x_i+\frac{h}{2}} \sin\sigma_{ih}x^* \sin\sigma_{jh}x^* \sin\sigma_{lh}x^* \sin\sigma_{mh}x^* \sin\sigma_{kh}x^*\, dx \tag{4-8f}$$

$$G_{ijlmnk} \equiv \int_{x_i-\frac{h}{2}}^{x_i+\frac{h}{2}} \sin\sigma_{ih}x^* \sin\sigma_{jh}x^* \sin\sigma_{lh}x^* \sin\sigma_{mh}x^* \sin\sigma_{nh}x^* \sin\sigma_{kh}x^*\, dx\,. \tag{4-8g}$$

In addition, we have the trivial system for k = 1:

$$\begin{bmatrix} \dot{a}_1 \\ \dot{b}_1 \\ \dot{c}_1 \\ \dot{d}_1 \\ \dot{e}_1 \end{bmatrix} = 0\,. \tag{4-9}$$

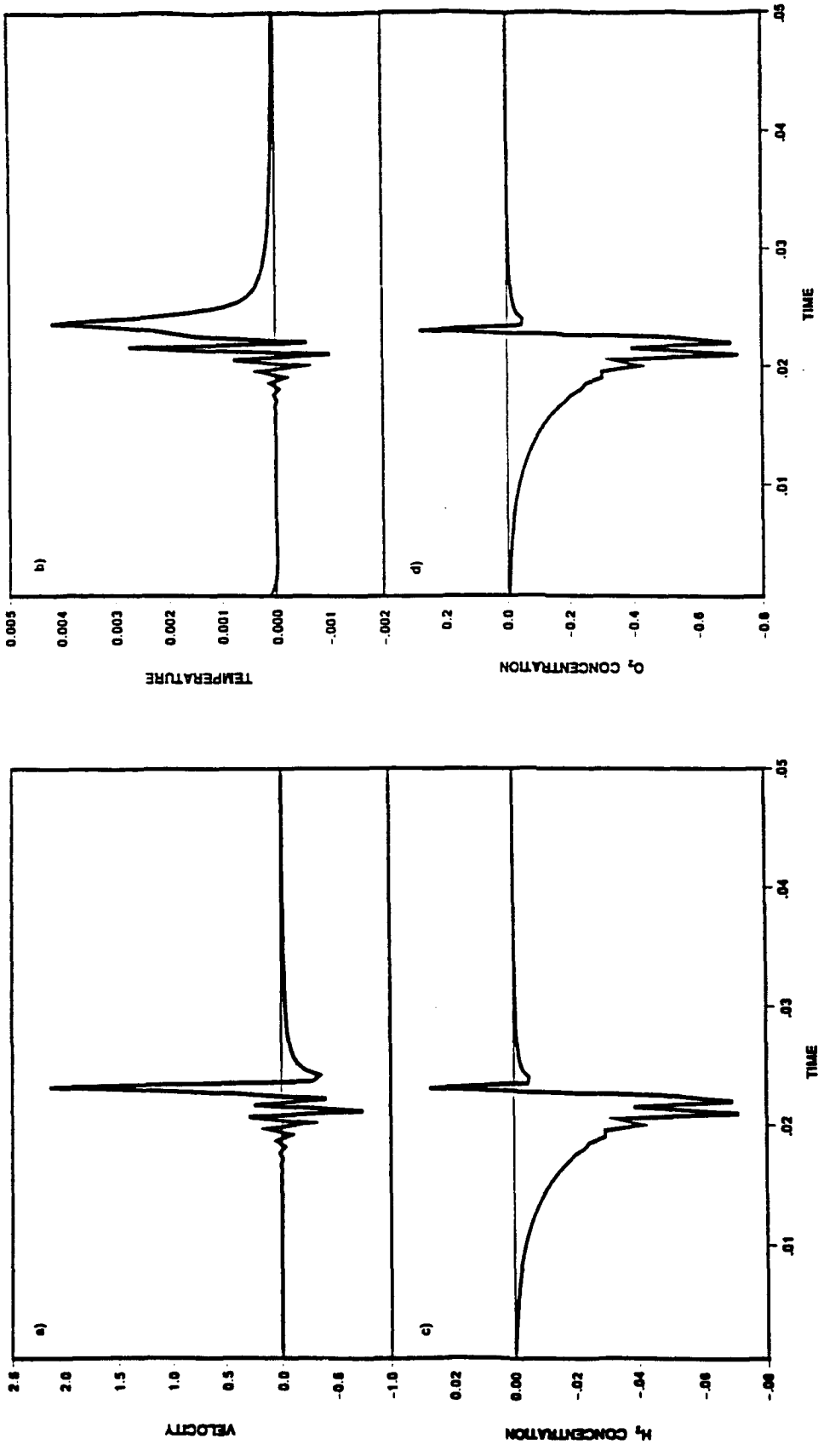


Figure 4-1 Small-Scale Fluctuations vs. Time: a) velocity, b) temperature, c) $H_2$ concentration, d) $O_2$ concentration

The Galerkin ODE's, Eqs. (4-6), are nonlinear and for large K can be expected to be stiff. Thus, one would typically expect to employ Gear's method as the solution technique. But because we are anticipating chaotic solutions (and hence, sensitivity to initial conditions), and because Gear's method is a multi-step method (with potential for parasitic error), we have chosen to employ a modification of the A-stable, single-step trapezoidal scheme. The modification consists of treating the nonlinear terms explicitly (via Heun's method), while maintaining implicit treatment of the linear terms, the main source of stiffness in this case. We of course do lose unconditional stability, but we also gain a significant reduction in the arithmetic that would be required to solve the linear systems that would have arisen in the application of Newton's method to the nonlinear terms had they been handled implicitly. This, in turn, reduces the round off error, which is highly desirable when integrating dynamical systems possessing chaotic solutions, again because of sensitivity to initial conditions.

Seven modes were retained in the small-scale representations of all dependent variables; i.e., K = 7. The dimensionless parameter values were Re = 6000, $Pe_T$ = 1000 and $Pe_D$ = 3000. Notice that we have not employed a Le = 1 assumption. The physical size of our small-scale region in the neighborhood of the flame tip was 0.5 mm. The dimensionless time step size employed in our numerical integrator was $\Delta t = 5.0\times10^{-4}$, corresponding to a physical time step of 0.666... μsec. The simulations were run for 100 time steps.

Results for velocity, temperature and $H_2$ and $O_2$ concentration fluctuations are displayed in Fig. 4-1. These were obtained by inserting the solutions to Eqs. (4-6) at each time t into Eqs. (4-5) and summing only from k = 2 to k = K. This construction starts with k = 2 because k = 1 is actually a Fourier mode corresponding to part of the large-scale solution.

There are a number of interesting observations to be made regarding Fig. 4-1. To begin, the temporal behavior on the small scale corresponds to what should be termed transient chaos. Careful examination of the figures shows that oscillatory behavior first begins in the small-scale velocity and temperature almost simultaneously. But this occurs only after a relatively long period of increase in negative amplitude of the $H_2$ and $O_2$ small-scale concentrations, which is consistent with depletion of reactants to form products. From Eq. (4-6b) we see that as the negative small-scale concentration amplitudes become large, they lead to positive forcing of the momentum equation, provided the large-scale local temperature gradient is positive. We have estimated this to have a value of 825 K/cm from data of Saito et al. [15]. Once the oscillations in velocity and temperature begin, they feed back into the species equations through the advective terms (for velocity), and the species production terms (for temperature.). It can also be seen that negative concentration fluctuations result in generally positive temperature fluctuations, as would be expected on physical grounds, since the negative concentration fluctuations imply product formation, and thus heat release. In general, these results appear to be generally consistent with expected physics.

## 5. MATHEMATICAL STUDIES RELATING TO ATD

Mathematical studies of techniques related to ATD were conducted at UCLA and focused on two issues. One focus was on a comparison of a technique for coupling the large scale and small scales in the 2D incompressible Navier-Stokes equations, to obtain efficient long time integrations. The other focus was on the development of fast solvers for elliptic problems in two dimensions, using domain decomposition techniques. Such solvers can be used to solve the linear systems arising from semi-implicit time stepping.

The original version of the ATD method was based on a decomposition of the solution into two scales, a large scale and a small scale component. Each component of the solution was computed by an iterative procedure. The studies at UCLA incorporated the recently developed non-linear Galerkin method proposed by Temam [16], Marion and Temam [17] and Titi [18], which was also based on a decomposition of the solution into two scales. However, the two scales were coupled through a stationary map which defined the small scale component in terms of the large scale component, in such a way that the resulting solution was on a non-linear manifold approximating the global attractor of the problem. The domain decomposition studies focused on a comparison of this technique for coupling the two scales with the standard pseudo-spectral method in which the two scales were coupled exactly.

Tests conducted for the 2D incompressible Navier-Stokes equations indicated that the non-linear Galerkin method can cost less than a corresponding pseudo-spectral method, due to the possibility of choosing larger time steps. The coupling used in [16] between the two scales resulted in good approximations, when the number of modes used to represent the large scale component was sufficiently large. However, the method developed some instabilties when the number of large scale modes was not sufficiently large. This restriction corresponded to the number of modes required to resolve the flow, as predicted by the theory of Henshaw, Kreiss and Reyna [19]. More tests are needed to study the possibilty of more efficient hybrid algorithms which adapts the number of modes used as the flow evolves into large scale structures.

The studies at UCLA on the development of fast solvers for elliptic problems, focused on using domain decomposition techniques with non-overlapping subdomains. Efficient versions of algorithms were developed having rates of convergence independent of mesh parameters, and also of coefficient variations, for symmetric positive definite elliptic problems in 2 dimensions. In some cases, the algorithms had a complexity of $O(N \log N)$, where N denotes the number of unknowns.

Details of these domain decomposition studies are presented in Appendix B.

## 6. SUMMARY OF WORK TO DATE

The work performed under the two grants — AFOSR 90-0271 and 89-0281 — has covered a range of subjects related to Additive Turbulent Decomposition. Work with Burgers' equation resulted in the development of a non-iterative algorithm for coupling the results of large-scale and small-scale time integrations, and the rigorous proof of its consistency and accuracy. These results were subsequently extended to the Navier-Stokes equations. A straightforward physical argument was found which determines a unique set of values for the decomposition tensors required when ATD is applied to the Navier-Stokes equations. A study of the effects of Reynolds averaging on the solution of Burgers' equation demonstrated that the ensemble average of the solution to the unaveraged equations equals the solution to the ensemble averaged equations if and only if properly averaged Reynolds stresses are used in the latter; and that the time average of the solution to the unaveraged equations is *never* exactly equal to the solution of the time averaged equations, even when exact Reynolds stresses are employed.

The 2-D small-scale equations have been implemented using a Chebyshev-tau method,

and applied used to examine the decay or growth of an isolated vortex. This problem is related to the origin of turbulence in shear flows. The results suggest that this problem is also related to the structure of wall-bounded flows, and tend to confirm the large body of experimental data associated with such flows. The code developed to examine this problem will be at the heart of a larger code implementing a highly parallel ATD algorithm we have defined for the Navier-Stokes equations. Work has begun on the application of ATD to the incompressible Navier-Stokes equations in 2-D generalized coordinates. The large-scale and small-scale equations, expressed in generalized coordinates, have been derived, and their implementation is in progress.

A number of mathematical studies have been carried out regarding ATD and domain decomposition. Two particular domain decomposition methods were studied in connection with ATD applied to Burgers' equation. The results showed that the Schwarz alternating method was more robust than the Gauss-Seidel-Newton (GSN) method, and required fewer iterations, but the arithmetic per iteration was much lower for the GSN method than for the Schwarz method. An approach related to ATD, the nonlinear Galerkin method of Temam [16], Marion and Temam [17] and Titi [18], was compared to the pseudo-spectral method of Henshaw, Kreiss and Reyna [19], and proved to be somewhat more efficient. And studies have been made of efficient and easily parallelizable methods for solving elliptic problems. These are especially applicable to the solution of the small-scale equations on the global domain.

Future work is expected to include the implementation of the complete ATD algorithm for the Navier-Stokes equations and its application to the problem of transition in channel flow, solution of the large-scale equations using a chaotic map to model the subgrid-scale effects, a parametric examination of the bifurcations in the solutions to the small-scale equations, and the development of a complete ATD code for generalized coordinates.

## PUBLICATIONS AND PRESENTATIONS

### Conference Presentations

Chan, T. F., at the Fifth International Conference on Domain Decomposition methods for Partial Differential Equations, Norfolk, VA, May 1991.

Chan, T. F., at the Oberwolfe Conference on Linear Algebra, Oberwolfe, April 1991.

Hylin, E.C. and McDonough, J.M., "Chaotic Motion on the Small Scale of the Navier-Stokes Equations," *Bull. Amer. Phys. Soc. 34,* 2251, 1989.

Matthew, T. P., at the Fifth International Conference on Domain Decomposition methods for Partial Differential Equations, Norfolk, VA, May 1991.

McDonough, J. M. "Investigation of Chemical Kinetics/Small-Scale Turbulence Interactions Via Additive Turbulent Decomposition," presented at the Workshop on Advances in Computational Methods for Transport Phenomena, Lexington, KY, Jan. 7-9, 1991.

McDonough, J. M., "The Large-Scale Equations of Additive Turbulent Decomposition as a Model of Chemically Reacting Turbulent Flow," presented at the XI$^{th}$ International Workshop on Mathematical Methods in Combustion," Tsukuba, Japan, July 26-27, 1991.

Peng, J.-S. and McDonough, J.M., "An Analysis of Reynolds Averaging Via a 1-D Burgers' Equation," *Bull. Amer. Phys. Soc. 34,* 2332, 1989.

### Refereed Conference Papers/Presentations

Chan, T. F. and Matthew, T. P., "An application of the probing technique to the vertex space method in domain decomposition," Tech. Report 90-22, UCLA, Department of Mathematics, Oct. 1990. Appeared in Proceedings of 4th International Conference on Domain Decomposition Methods, Moscow, May 1990. SIAM.

Hylin, E.C. and McDonough, J.M., "Additive Turbulent Decomposition Applied to an Isolated Vortex in a Constant Shear Flow," to be presented at 4$^{th}$ International Symposium on Computational Fluid Dynamics, Davis, CA, Sep. 9-12, 1991.

McDonough, J. M. and Peng, J.-S., "A Numerical Study of Reynolds Averaging Via Burgers' Equation with Chaotic Forcing," to be submitted for presentation at the 2$^{nd}$ National Fluid Dynamics Congress, Los Angeles, CA, June 22-25, 1992.

McDonough, J. M. and Saito, K. "Local, Small-Scale Interaction of Turbulence with Chemical Reactions in $H_2$-$O_2$ Combustion," presented at 13$^{th}$ International Colloquium on the Dynamics of Explosions and Reactive Systems, Nagoya, Japan, Jul. 28 - Aug. 2, 1991.

### Other Papers

Chan, T. F. and Matthew, T. P., "The interface probing technique in domain decomposition," Tech. Report 91-02, UCLA, Department of Mathematics, Feb. 1991. To appear in SIAM Journal on Matrix Analysis.

Chan, T. F., Matthew, T. P., and Shao, J-P, "Some domain decomposition algorithms for self-adjoint elliptic problems," under preparation.

Chan, et al., also plan to write a paper based on their studies of the ATD method and the nonlinear Galerkin method.

### Invited Talks and Lectures

McDonough, J. M., "Effects of Reynolds Averaging Applied to Quasilinear Parabolic PDE's," presented at University of Kentucky Mathematics Seminar, Lexington, KY, April 25, 1991.

McDonough, J. M., "Effects of Reynolds Averaging Applied to Quasilinear Parabolic PDE's," presented at NIST, Gaithersburg, MD, July 2, 1991.

McDonough, J. M. "Additive Turbulent Decomposition: A New Direction in Turbulence Simulation -- An Overview," presented at the University of Tokyo, Tokyo, Japan, July 25, 1991.

### Masters Theses

Peng, J.-S., "An Analysis of Reynolds Averaging via One-dimensional Burgers' Equation," Mechanical, Aerospace and Nuclear Engineering, University of California, Los Angeles, 1990.

## REFERENCES


1. J. M. McDonough, R. J. Bywater, and J. C. Buell, AIAA Paper 84-1674, 1984.

2. J. M. McDonough, E. C. Hylin, Ivan Catton, Tony F. C. Chan and T. Matthew, Annual Report for AFOSR Grant 89-0281, submitted 30 October 1989.

3. J. Kim and P. Moin, *J. Comput. Phys. 59*, 308-323, 1985.

4. J. Douglas and J. E. Gunn, *Numer. Math. 6*, 428-453, 1964.

5. J. M. McDonough, E. C. Hylin, Tony F. C. Chan and T. Matthew, Annual Report for AFOSR Grant 90-0271, submitted 31 October 1990.

6. D. B. Haidvogel and T. Zang, *J. Comput. Phys. 30*, 167-180, 1979.

7. C. Canuto, M. Y. Hussaini, A. Quarteroni and T. A. Zang, *Spectral Methods in Fluid Dynamics*, Springer-Verlag, New York, 1988.

8. P. M. Gresho and R. L. Sani, *Int. J. Num. Meth. Fluids, 7*, 1111-1145, 1987.

9. P. M. Gresho, *Int. J. Num. Meth. Fluids, 11*, 587-620, 1990.

10. J. M. McDonough, E. C. Hylin, Ivan Catton, Tony F. C. Chan and T. Matthew, Final Report for AFOSR Grant 89-0281, submitted 30 May 1990.

11. T. F. Chan and T. P. Matthew, *An application of the probing technique to the vertex space method in domain decomposition*, Tech. Report 90-22, UCLA, Department of Mathematics, Oct. 1990. Appeared in Proceedings of 4th International Conference on Domain Decomposition Methods, Moscow, May 1990. SIAM.

12. T. F. Chan and T. P. Matthew, *The interface probing technique in domain decomposition*, Tech. Report 91-02, UCLA, Department of Mathematics, Feb. 1991. To appear in SIAM Journal on Matrix Analysis.

13. S. A. Orszag and M. D. Kruskal, *Phy. Fluids, 11*, 43-60, 1968.

14. J. M. McDonough and K. Saito, *Local, small-scale interaction of turbulence with chemical reactions in $H_2$-$O_2$ combustion*, presented at the 13th International Colloquium on the Dynamics of Explosions and Reactive Systems, Nagoya, Japan, 28 July - 2 August, 1991.

15. K. Saito, F. A. Williams and A. S. Gordon, *ASME J. Heat Transfer 108*, 640, 1986.

16. R. Temam, *The nonlinear Galerkin method in computational fluid dynamics*, To appear.

17. M. Marion and R. Temam, *SIAM J. Numer. Anal., 26(5)*, 1139-1157, 1989.

18. E. S. Titi, *J. Math. Anal. & Appl., 149(2)*, 1990.

19. W. D. Henshaw, H.-O. Kreiss and L. G. Reyna, *On the smallest scale for the incompressible Navier-Stokes equations*, CAM Report 88-10, UCLA, Department of Mathematics, March 1988.

# APPENDIX A: Derivation of the ATD Equations in Generalized Coordinates

## APPENDIX A: DERIVATION OF THE ATD EQUATIONS IN GENERALIZED COORDINATES

### A.1 Derivation of the Large-Scale Momentum Equations in Generalized Coordinates

With the pressure-gradient terms omitted, the Navier-Stokes momentum equations in 2-D cartesian coordinates are:

$$\frac{\partial u}{\partial t} + \frac{\partial}{\partial x}(u^2) + \frac{\partial}{\partial y}(vu) = \frac{1}{Re}\Delta u \tag{A-1}$$

$$\frac{\partial v}{\partial t} + \frac{\partial}{\partial x}(uv) + \frac{\partial}{\partial y}(v^2) = \frac{1}{Re}\Delta v \tag{A-2}$$

Define a general coordinate transformation T such that

$$(x_1, x_2) \leftarrow T \rightarrow (\xi_1, \xi_2) \tag{A-3}$$

We can apply this transformation to equations A-1 and A-2 and, using the chain rule for derivatives, obtain the corresponding equations in generalized coordinates:

$$\begin{aligned}
&\frac{\partial}{\partial t}\left(\frac{u}{J}\right) + \left\{\left[\frac{1}{J}(\xi_x u^2 + \xi_y uv)\right]_\xi + \left[\frac{1}{J}(\eta_x u^2 + \eta_y uv)\right]_\eta\right\} \\
&\quad - \frac{1}{Re}\left\{\left[\frac{1}{J}\left(\xi_x^2\frac{\partial u}{\partial \xi} + \xi_x\eta_x\frac{\partial u}{\partial \eta} + \xi_y\eta_y\frac{\partial u}{\partial \eta} + \xi_y^2\frac{\partial u}{\partial \eta}\right)\right]_\xi\right\} \\
&\quad - \frac{1}{Re}\left\{\left[\frac{1}{J}\left(\eta_x^2\frac{\partial u}{\partial \eta} + \xi_x\eta_x\frac{\partial u}{\partial \xi} + \xi_y\eta_y\frac{\partial u}{\partial \xi} + \eta_y^2\frac{\partial u}{\partial \eta}\right)\right]_\eta\right\} = 0
\end{aligned} \tag{A-4}$$

and

$$\begin{aligned}
&\frac{\partial}{\partial t}\left(\frac{v}{J}\right) + \left\{\left[\frac{1}{J}(\xi_x uv + \xi_y v^2)\right]_\xi + \left[\frac{1}{J}(\eta_x uv + \eta_y v^2)\right]_\eta\right\} \\
&\quad - \frac{1}{Re}\left\{\left[\frac{1}{J}\left(\xi_x^2\frac{\partial v}{\partial \xi} + \xi_x\eta_x\frac{\partial v}{\partial \eta} + \xi_y\eta_y\frac{\partial v}{\partial \eta} + \xi_y^2\frac{\partial v}{\partial \eta}\right)\right]_\xi\right\} \\
&\quad - \frac{1}{Re}\left\{\left[\frac{1}{J}\left(\eta_x^2\frac{\partial v}{\partial \eta} + \xi_x\eta_x\frac{\partial v}{\partial \xi} + \xi_y\eta_y\frac{\partial v}{\partial \xi} + \eta_y^2\frac{\partial v}{\partial \eta}\right)\right]_\eta\right\} = 0
\end{aligned} \tag{A-5}$$

Where

$$\frac{1}{J}=\begin{bmatrix}\frac{\partial x_1}{\partial \xi_1} & \frac{\partial x_1}{\partial \xi_2}\\ \frac{\partial x_2}{\partial \xi_1} & \frac{\partial x_2}{\partial \xi_2}\end{bmatrix} \quad \text{and} \quad J=\begin{bmatrix}\frac{\partial \xi_1}{\partial x_1} & \frac{\partial \xi_1}{\partial x_2}\\ \frac{\partial \xi_2}{\partial x_1} & \frac{\partial \xi_2}{\partial x_2}\end{bmatrix}$$

Using the particular decomposition described by Hylin in McDonough, et al. [A-1], large-scale momentum equations corresponding to equations A-1 and A-2 are

$$\frac{\partial u}{\partial t}+\frac{\partial}{\partial x}(u^2)+\frac{\partial}{\partial y}(vu)+\frac{\partial}{\partial x}(u^*u)+\frac{\partial}{\partial y}(v^*u)=\frac{1}{Re}\Delta u \tag{A-6}$$

$$\frac{\partial v}{\partial t}+\frac{\partial}{\partial x}(uv)+\frac{\partial}{\partial y}(v^2)+\frac{\partial}{\partial x}(u^*v)+\frac{\partial}{\partial y}(v^*v)=\frac{1}{Re}\Delta v \tag{A-7}$$

where u* and v* denote the small-scale velocities. In generalized coordinates, these equations become:

$$\begin{aligned}&\frac{\partial}{\partial t}\left(\frac{u}{J}\right)+\left\{\left[\frac{1}{J}(\xi_x u^2+\xi_y vu)\right]_\xi+\left[\frac{1}{J}(\eta_x u^2+\eta_y vu)\right]_\eta\right\}\\ &\quad+\left\{\left[\frac{1}{J}(\xi_x u^*u+\xi_y v^*u)\right]_\xi+\left[\frac{1}{J}(\eta_x u^*u+\eta_y v^*u)\right]_\eta\right\}\\ &\quad-\frac{1}{Re}\left\{\left[\frac{1}{J}\left(\xi_x^2\frac{\partial u}{\partial \xi}+\xi_x\eta_x\frac{\partial u}{\partial \eta}+\xi_y\eta_y\frac{\partial u}{\partial \eta}+\xi_y^2\frac{\partial u}{\partial \eta}\right)\right]_\xi\right\}\\ &\quad-\frac{1}{Re}\left\{\left[\frac{1}{J}\left(\eta_x^2\frac{\partial u}{\partial \eta}+\xi_x\eta_x\frac{\partial u}{\partial \xi}+\xi_y\eta_y\frac{\partial u}{\partial \xi}+\eta_y^2\frac{\partial u}{\partial \eta}\right)\right]_\eta\right\}=0\end{aligned} \tag{A-8}$$

and

$$\begin{aligned}&\frac{\partial}{\partial t}\left(\frac{v}{J}\right)+\left\{\left[\frac{1}{J}(\xi_x uv+\xi_y v^2)\right]_\xi+\left[\frac{1}{J}(\eta_x uv+\eta_y v^2)\right]_\eta\right\}\\ &\quad+\left\{\left[\frac{1}{J}(\xi_x u^*v+\xi_y v^*v)\right]_\xi+\left[\frac{1}{J}(\eta_x u^*v+\eta_y v^*v)\right]_\eta\right\}\\ &\quad-\frac{1}{Re}\left\{\left[\frac{1}{J}\left(\xi_x^2\frac{\partial v}{\partial \xi}+\xi_x\eta_x\frac{\partial v}{\partial \eta}+\xi_y\eta_y\frac{\partial v}{\partial \eta}+\xi_y^2\frac{\partial v}{\partial \eta}\right)\right]_\xi\right\}\\ &\quad-\frac{1}{Re}\left\{\left[\frac{1}{J}\left(\eta_x^2\frac{\partial v}{\partial \eta}+\xi_x\eta_x\frac{\partial v}{\partial \xi}+\xi_y\eta_y\frac{\partial v}{\partial \xi}+\eta_y^2\frac{\partial v}{\partial \eta}\right)\right]_\eta\right\}=0\end{aligned} \tag{A-9}$$

The underscored terms are those involving the small-scale velocities u* and v*, and do not appear in equations A-4 and A-5. We will be developing a chaotic map to model u* and v*, with the expectation that the large-scale equations derived via ATD and used in conjunction with such a map may be able to simulate more general turbulent flows than is possible with LES and the current models for subgrid-scale effects.

In discretizing equations A-8 and A-9, we first linearize them by means of the δ-form quasilinearization, then rearrange the equations to make the diffusive and convective terms clearer. For the spatial discretization we use the standard staggered grid, with centered differencing for the diffusive terms and first-order upwinding for the convective terms.

### A.2 Derivation of the Small-Scale Momentum Equations in Generalized Coordinates

As derived by Hylin in McDonough, et al. [A-1], the small-scale momentum equation is

$$\frac{\partial \mathbf{u}^*}{\partial t} = \frac{1}{Re}\Delta \mathbf{u}^* - \nabla\cdot(\mathbf{u}\mathbf{u}^*) - \nabla\cdot(\mathbf{u}^*\mathbf{u}^*) - \nabla p^* \tag{A-10}$$

while in generalized coordinates, the momentum equations are in the form

$$Q_t + F_\xi + G_\eta = \frac{1}{Re}(R_{\xi\xi} + S_{\xi\eta} + T_{\eta\eta}), \tag{A-11}$$

as given by Fletcher [A-2]. The contravariant velocities U and V are defined to be

$$U = \xi_x u + \xi_y v \qquad V = \eta_x u + \eta_y v, \tag{A-12}$$

where $\xi_x$, $\eta_y$, etc. are elements of the Jacobian matrix of the coordinate transformation. The momentum equations contain both contravariant velocities and primitive velocities and in terms of these velocities the terms in the small-scale version of equation A-11 become

$$Q = \frac{1}{J^2}\begin{bmatrix} \eta_y U^* - \xi_y V^* \\ \xi_x V^* - \eta_x U^* \end{bmatrix} \tag{A-13a}$$

$$F = \frac{1}{J}\begin{bmatrix} \frac{1}{J}(\eta_y U^* - \xi_y V^*)(U^* + U + \frac{\xi_{xx} + \xi_{yy}}{Re}) + \xi_x p^* \\ \frac{1}{J}(\xi_x V^* - \eta_x U^*)(U^* + U + \frac{\xi_{xx} + \xi_{yy}}{Re}) + \xi_x p^* \end{bmatrix} \tag{A-13b}$$

$$G = \frac{1}{J}\begin{bmatrix} \frac{1}{J}(\eta_y U^* - \xi_y V^*)(V^* + V + \frac{\eta_{xx} + \eta_{yy}}{Re}) + \eta_x p^* \\ \frac{1}{J}(\xi_x V^* - \eta_x U^*)(V^* + V + \frac{\eta_{xx} + \eta_{yy}}{Re}) + \eta_y p^* \end{bmatrix} \tag{A-13c}$$

$$R = \frac{1}{J^2}\begin{bmatrix} (\xi^2_x + \xi^2_y)(\eta_y U^* - \xi_y V^*) \\ (\xi^2_x + \xi^2_y)(\xi_x V^* - \eta_x U^*) \end{bmatrix} \tag{A-13d}$$

$$S = \frac{1}{J^2}\begin{bmatrix}(2\xi_x\eta_x + \xi_y\eta_y)(\eta_y U^* - \xi_y V^*)\\ (2\xi_x\eta_x + \xi_y\eta_y)(\xi_x V^* - \eta_x U^*)\end{bmatrix} \qquad \text{(A-13e)}$$

$$T = \frac{1}{J^2}\begin{bmatrix}(\eta_x^2 + \eta_y^2)(\eta_y U^* - \xi_y V^*)\\ (\eta_x^2 + \eta_y^2)(\xi_x V^* - \eta_x U^*)\end{bmatrix} \qquad \text{(A-13f)}$$

where U and V are the large-scale contravariant velocities.

To construct the local approximation, we consider a cell centered at $(\xi_i, \eta_i)$, and assume the solution can be represented by truncated Fourier series, defined as follows,

$$U^*(\xi,\eta,t) = J\sum_{k,l}^{K} a(t)_{kl}\cos\alpha_k\frac{\xi-\bar{\xi}_i}{h}\sin\alpha_l\frac{\eta-\bar{\eta}_i}{h} \qquad \text{(A-14a)}$$

$$V^*(\xi,\eta,t) = J\sum_{k,l}^{K} b_{kl}(t)\sin\alpha_k\frac{\xi-\bar{\xi}_i}{h}\cos\alpha_l\frac{\eta-\bar{\eta}_i}{h} \qquad \text{(A-14b)}$$

$$p^*(\xi,\eta,t) = \sum_{k,l}^{K} c_{kl}(t)\sin\alpha_k\frac{\xi-\bar{\xi}_i}{h}\sin\alpha_l\frac{\eta-\bar{\eta}_i}{h} \qquad \text{(A-14c)}$$

where

$$\bar{\xi}_i = \xi_i - \frac{h}{2}, \quad \bar{\eta}_i = \eta_i - \frac{h}{2},$$

$$\alpha_k = k\pi, \qquad \alpha_l = l\pi,$$

and h is the finite difference grid spacing for the large-scale calculation. We now substitute Eq.(A-14) into (A-13) and construct the Galerkin inner products. The resulting system of ordinary differential equations for the time-dependent Fourier coefficients is

$$\frac{1}{J}\eta_y\dot{a}_{kl} = \frac{f_{kl}}{C_1C_2} + \xi_x k c_{kl} + \frac{d}{d\xi}\left[\frac{\eta_y}{J}\left(U + \frac{\xi_{xx}+\xi_{yy}}{Re}\right)\right]a_{kl}$$

$$+ \frac{d}{d\eta}\left[\frac{\eta_y}{J}\left(V + \frac{\eta_{xx}+\eta_{yy}}{Re}\right)\right]a_{kl} \qquad \text{(A-15a)}$$

$$+ \frac{1}{Re}\left\{\frac{d^2}{d\xi^2}\left[\frac{\eta_y}{J}\left(\xi_x^2+\xi_y^2\right)\right] - \left(\frac{k\pi}{h}\right)^2\frac{\eta_y}{J}\left(\xi_x^2+\xi_y^2\right)\right\}a_{kl}$$

$$+ \frac{1}{Re}\left\{\frac{d^2}{d\eta^2}\left[\frac{\eta_y}{J}\left(\eta_x^2+\eta_y^2\right)\right] - \left(\frac{l\pi}{h}\right)^2\frac{\eta_y}{J}\left(\eta_x^2+\eta_y^2\right)\right\}a_{kl}$$

$$\frac{1}{J}\xi_x \dot{b}_{kl} = \frac{g_{kl}}{C_1 C_2} + \eta_y lc_{kl} + \frac{d}{d\xi}\left[\frac{\xi_x}{J}(U + \frac{\xi_{xx}+\xi_{yy}}{Re}\right]b_{kl}$$

$$+ \frac{d}{d\eta}\left[\frac{\xi_x}{J}(V + \frac{\eta_{xx}+\eta_{yy}}{Re}\right]b_{kl} \qquad \text{(A-15b)}$$

$$+ \frac{1}{Re}\left\{\frac{d^2}{d\xi^2}\left[\frac{\xi_x}{J}\left(\xi_x^2+\xi_y^2\right)\right] - \left(\frac{k\pi}{h}\right)^2 \frac{\xi_y}{J}\left(\xi_x^2+\xi_y^2\right)\right\}b_{kl}$$

$$+ \frac{1}{Re}\left\{\frac{d^2}{d\eta^2}\left[\frac{\xi_x}{J}\left(\eta_x^2+\eta_y^2\right)\right] - \left(\frac{l\pi}{h}\right)^2 \frac{\eta_y}{J}\left(\eta_x^2+\eta_y^2\right)\right\}b_{kl}$$

where

$$C_1 = \int\int \sin^2 \frac{\xi - \xi_i}{h}\, d\xi d\xi\,, \quad C_2 = \int\int \cos^2 \frac{\eta - \eta_i}{h}\, d\eta d\eta\,,$$

and $f_{kl}$ and $g_{kl}$ are the Galerkin inner products of the nonlinear terms:

$$-f_{kl} = \frac{d\eta_y}{d\xi}\sum_{i,j,m,n}^{K} a_{ij}a_{mn}A_{kim}B_{ljn} + \eta_y \sum_{i,j,m,n}^{K} \frac{\pi}{h} a_{ij}a_{mn}(-iC_{kim} + mC_{kmi})B_{ljn}$$

$$- \frac{d\xi_y}{d\xi}\sum_{i,j,m,n}^{K} b_{ij}a_{mn}C_{kim}D_{ljn} - \xi_y \sum_{i,j,m,n}^{K} \frac{\pi}{h} b_{ij}a_{mn}(iA_{kim} - mD_{imk})D_{lnj} \qquad \text{(A-16a)}$$

$$+ \frac{d\eta_y}{d\eta}\sum_{i,j,m,n}^{K} a_{ij}b_{mn}C_{kim}D_{ljn} + \eta_y \sum_{i,j,m,n}^{K} \frac{\pi}{h} a_{ij}b_{mn}C_{kmi}(jC_{kim} - nB_{ljn})$$

$$- \frac{d\xi_y}{d\eta}\sum_{i,j,m,n}^{K} b_{ij}b_{mn}D_{imk}C_{jln} - \xi_y \sum_{i,j,m,n}^{K} \frac{\pi}{h} b_{ij}b_{mn}D_{imk}(-jD_{ljn} - nD_{lnj})$$

$$
\begin{aligned}
-g_{kl} = {} & \frac{d\xi_x}{d\xi}\sum_{i,j,m,n}^{K} b_{ij}a_{mn}D_{kim}C_{ljn} + \xi_x\sum_{i,j,m,n}^{K}\frac{\pi}{h}b_{ij}a_{mn}(-iC_{ikm} - mB_{kim})C_{lnj} \\
& - \frac{d\eta_x}{d\xi}\sum_{i,j,m,n}^{K} a_{ij}a_{mn}C_{ikm}D_{jnl} - \eta_x\sum_{i,j,m,n}^{K}\frac{\pi}{h}a_{ij}a_{mn}(-jD_{kim} - mD_{kmi})D_{jnl} \qquad \text{(A-16b)} \\
& + \frac{d\xi_x}{d\eta}\sum_{i,j,m,n}^{K} b_{ij}b_{mn}B_{kim}A_{ljn} + \xi_x\sum_{i,j,m,n}^{K}\frac{\pi}{h}b_{ij}b_{mn}B_{kim}(-jD_{ljn} - nD_{lnj}) \\
& - \frac{d\eta_x}{d\eta}\sum_{i,j,m,n}^{K} a_{ij}b_{mn}D_{kmi}C_{ljn} - \eta_x\sum_{i,j,m,n}^{K}\frac{\pi}{h}a_{ij}b_{mn}D_{kmi}(-jA_{ljn} - nD_{jnl})
\end{aligned}
$$

## References


1. J. M. McDonough, E .C. Hylin, Ivan Cattan, Tony F. C. Chan and T. Mathew, Annual Report for AFOSR Grant 89-0271, Submitted 30 Oct 1989.

2. C. A. J. Fletcher, *Computational Techniques for Fluid Dynamics 2,* Springer-Verlag, New York, 1988

# APPENDIX B: Mathematical Studies Relating to ATD

**FINAL REPORT ON**

Studies of the Additive Turbulent Decomposition Method.

Supported by AFOSR Grant 90-0271, subcontract to UCLA
from University of Kentucky UKRF-4-24384-90-87

*by Tony F. Chan and Tarek Mathew*
Department of Mathematics, UCLA.

# 1 Introduction

This project concerns a study of some techniques for efficiently integrating the incompressible Navier-Stokes equations over large time intervals. For such problems, with time independent forcing, turbulent solutions may converge in function space to a finite dimensional set referred to as the global attractor, see [4]. In this case, the long term behaviour of the solutions can essentially be described by a finite dimensional sytem of ODE's which captures the large scale properties of the global attractor. Thus far, however, computing accurate solutions of the incompressible Navier-Stokes equations by direct simulation is still very expensive, especially in three dimensions. Some alternate techniques have been proposed which reduces this cost, such as Large Eddy Simulation techniques (LES), see [5] [6]. Recently, the Additive Turbulent Decomposition method (ATD) was proposed by McDonough and Bywater [9] [10] as an alternative direct simulation technique without the use of statistical parameters. In this report, we breifly describe our studies on the ATD method and related methods for numerically integrating the incompressible Navier-Stokes equations over large intervals of time.

We compare two approaches. In one case, we follow a method related to the basic idea in the original version of the ATD method proposed in [9, 10], which was, to decompose the solution as a sum of a large scale and small scale component and to approximately determine each component by an iterative technique based on the original equations. Our studies led us to incorporate the coupling used in the recently developed non-linear Galerkin method of Temam [13], Marion and Temam [8] and Titi [14]. The non-linear Galerkin method is also based on a splitting of the solution into two components, large scale and small scale. However, unlike the coupling used in the original ATD version, the coupling between the large scale and small scale terms

is determined by a stationary mapping which defines the small scale component in terms of the large scale component. We use this form of coupling between the two scales.

In another approach, we use a pseudo-spectral method of Henshaw, Kreiss and Reyna [7], in which the number of modes used is chosen to provide a convergent numerical approximation. This is based on a theory for the minimum scale of the flow, presented in [7]. The minimum scale can also be used to *adapt* the number of modes required to resolve the flow, as the flow evolves into coherent structures, therby leading to improved efficiency. In Section 5, we compare the non-linear Galerkin method with the pseudo-spectral method. Our studies are restricted to the vorticity-stream function formulation of the 2D incompressible Navier-Stokes equations on a periodic domain,

The rest of the report is outlined as follows. We describe the vorticity-stream function formulation of the incompressible Navier-Stokes equations on a periodic domain in 2 dimensions. We then describe its discretisation by a pseudo-spectral method in space and a 4th order predictor corrector in time. Following that we describe the non-linear Galerkin method. We present some numerical comparisons of the two methods considered and some of their properties are discussed. Finally, we report on some related work we have done on developing fast solvers for elliptic problems using domain decomposition techniques. Such algorithms can be applied to solve the linear systems obtained when semi-implicit time stepping is used for non-periodic boundary conditions.

# 2 Navier-Stokes equations in two dimensions

The velocity-pressure formulation of the 2 dimensional incompressible Navier-Stokes equations on the square $[0, 2\pi] \times [0, 2\pi]$ with periodic boundary conditions reads:

$$\begin{array}{lcll} \mathbf{u}_t + u\mathbf{u}_x + v\mathbf{u}_y + \nabla p & = & \nu\Delta\mathbf{u} + \mathbf{f} & \text{in } [0,2\pi]^2 \\ \nabla \cdot \mathbf{u} & = & 0 & \text{in } [0,2\pi]^2 \\ \mathbf{u}(t=0,.) & = & \mathbf{u}_0 & \text{for t} = 0 \end{array} \qquad (1)$$

where $\mathbf{u} = (u, v)$ denotes the velocity, $p$ denotes the pressure, $\mathbf{f}$ denotes a time independent forcing, and $\nu$ denotes the kinematic viscosity. The vorticity $\omega \equiv \nabla \times \mathbf{u}$

satisfies:

$$\begin{aligned} \omega_t + u\omega_x + v\omega_y &= \nu\omega + f \\ \omega(t=0,x,y) &= \omega_0(x,y) \end{aligned} \tag{2}$$

where $(u,v) = \mathbf{u} = (\psi_y, -\psi_x)$ is the curl of the stream function $\psi$ which satisfies:

$$-\Delta\psi = \omega.$$

Thus, in the 2 dimensional case, $u$, $v$ and $\psi$ are determined by the vorticity and we will consider the solution of scalar evolution equation (2) for $\omega$.

# 3 A pseudo-spectral method

We now describe a pseudo-spectral method used in Henshaw, Kreiss and Reyna [7], and Browning and Kreiss [2], which leads to convergent numerical approximations for the vorticity equation (2). In the pseudo spectral method, the solution $\omega$ is approximated by a truncated Fourier series $\omega_N$, whose coefficients (which depend on time) evolves as a system of ODE's:

$$\omega(t,x,y) \approx \omega_N(t,x,y) = \sum_{k_1,k_2=-N/2+1}^{N/2-1} \hat{\omega}(t,k_1,k_2) e^{i(k_1 x + k_2 y)},$$

where, for each $\mathbf{k}= (k_1,k_2)$, the Fourier coefficient $\hat{\omega}(t,k_1,k_2)$ satisfies:

$$\hat{\omega}_t(t,\mathbf{k}) + \widehat{u\omega_x}(t,\mathbf{k}) + \widehat{v\omega_y}(t,\mathbf{k}) + \nu|\mathbf{k}|^2\hat{\omega}(t,\mathbf{k}) = \hat{f}(\mathbf{k}).$$

The ODE system can be written:

$$\hat{w}_t + \nu\Lambda\hat{w} = G(\hat{w}),$$

where $G(\hat{w}) = -\widehat{uw_x} - \widehat{vw_y} + \hat{f}$ represents the convection term and the forcing, and $\Lambda$ is a diagonal matrix with entries: $\Lambda_{\mathbf{k}} = |\mathbf{k}|^2$.

In our tests, the ODE system for the coefficients $\hat{\omega}(\mathbf{k})$ were integrated by the use of a 4th order Predictor-Corrector method, as in [7], in which the diffusion term was integrated exactly. For time step $\Delta t$ the prediction step reads:

$$\hat{w}_p = e^{-\nu\Lambda\Delta t}\hat{w}_n + \frac{\Delta t}{12}\left(23e^{-\nu\Lambda\Delta t}G_n - 16e^{-2\nu\Lambda\Delta t}G_{n-1} + 5e^{-3\nu\Lambda\Delta t}G_{n-2}\right),$$

and the correction step:

$$\hat{w}_{n+1} = e^{-\nu\Lambda\Delta t}\hat{w}_n + \frac{\Delta t}{24}\left(9G_p + 19e^{-\nu\Lambda\Delta t}G_n - 5e^{-2\nu\Lambda\Delta t}G_{n-1} + e^{-3\nu\Lambda\Delta t}G_{n-2}\right).$$

In our tests, for mesh parameter $\tilde{h} \equiv 2/N$, the time step $\Delta t$ was chosen to satisfy the following CFL condition:

$$CFL_{min} \leq (|u|_\infty + |v|_\infty) \frac{\Delta t}{\tilde{h}} \leq CFL_{max},$$

where $CFL_{min}$ was chosen to be 0.1 and $CFL_{max}$ was chosen to be 1.2. So long as the choice of $\Delta t$ kept the CFL quantity within the bounds, the step size was not altered. But when it fell outside the range, the new time step was chosen to be:

$$\Delta t_{new} = \frac{0.5\tilde{h}}{(|u|_\infty + |v|_\infty)}.$$

The cost of evaluating the derivitive $\omega_t$ is roughly proportional to the cost of computing the convolution term. This can be evaluated approximately using 5 two dimensional FFT's by mapping $\hat{\omega_x}$, $\hat{\omega_y}$, $\hat{u}$ and $\hat{v}$ to real space, forming $u\omega_x + v\omega_y$ in real space, and mapping the result back to Fourier space (pseudo-spectral method).

The theory of Henshaw, Kreiss and Reyna [7] gives an explicit bound for the maximum number of modes $N_{max}$ needed to resolve the flow:

$$N_{max} \leq C \left( \frac{|Du|_\infty}{\nu} \right)^{1/2},$$

where $\nu$ is the kinematic viscosity and $|Du|_\infty$ is the maximum of the velocity gradients for the flow, for all time, if that is known *a priori*. Over large time intervals, as the flow evolves into large scale structures, it would be possible to adapt $N_{max}$ for improved efficiency, by using the above estimate. We intend on testing the efficiency of adaptive gridding.

# 4 Non-linear Galerkin method

As mentioned earlier, our studies of the coupling between the two scales in the original version of the ATD method, led us to consider an alternate form of coupling used in the non-linear Galerkin method of Marion and Temam [8] and Titi [14]. We have used this coupling in the tests reported here. We now briefly describe the nonlinear Galerkin method for an evolution equation in a function space $H$:

$$\begin{aligned} &w_t + \nu A w + B(w) = f \\ &w(0) = w_0 \end{aligned} \tag{3}$$

where $A$ denotes a self-adjoint positive operator on $H$ (such as $-\Delta$), $\nu$ denotes a small parameter, $B(w)$ is a nonlinear map (such as $uw_x + vw_y$), and $f$ is a time independent forcing. The function space is decomposed $H = H^L + H^S$, where $H^L$ represents the space spanned by some large scale eigenfunctions of $A$ and $H^S$ represents its orthogonal complement. The solution $w$ can be decomposed $w = p + q$, where $p \in H^L$ and $q \in H^S$. Equation (3) is then equivalent to the coupled system:

$$\begin{aligned} p_t + \nu Ap + P_L B(p+q) &= P_L f \\ q_t + \nu Aq + P_S B(p+q) &= P_S f \end{aligned} \tag{4}$$

where $P_L$ denotes orthogonal projection onto $H_L$ and $P_S = I - P_L$. In the original version of the ATD method, system (4) was solved by means of an iterative procedure. However, in the non-linear Galerkin method, under the assumption that $\|q\| \ll \|p\|$ and $\|q_t\| \ll \|\nu Aq + P_S(B(p) - f)\|$, the 2nd equation in (4) is approximated by:

$$\nu Aq + P_S B(p) = P_S f,$$

which defines the small scale component $q$ in terms of the large scale component $p$, by a function $\Phi(p)$ defined by

$$q = \Phi(p) = (\nu A)^{-1} P_S \left(f - B(p)\right). \tag{5}$$

The resulting new system for the large scale component $p$ reads.

$$p_t + \nu Ap + P_L B(p + \Phi(p)) = P_L f \tag{6}$$

Equation (6) comprises the nonlinear Galerkin method for $p$, and is different from the standard Galerkin equations for $p$: it includes the nonlinear coupling between the two scales. For each $p$, its corresponding small scale component $\Phi(p)$ can be determined using (5), thereby leading to a solution in $H_L + H_S$.

In our application, the space $H \subset L^2([0, 2\pi] \times [0, 2\pi])$ corresponds to the Fourier modes of wavenumbers less than $N$, $H_L$ corresponds to Fourier modes of wavenumbers less than $N/2$ and $H_S$ corresponds to the remaining Fourier modes in $H$. In the tests, we discretised evolution equation (6) for the large scale component $p$, by an application of the pseudo-spectral method. We note that the method described here can also be extended to the case where finite difference or finite element discretisations are used, as has been reported in the 1991 ICIAM conference.

# 5 Numerical Tests

We present here the results of a sample test comparing the performance of the non-linear Galerkin method with the standard pseudo-spectral method, as described in Sections 3 and 4. In particular, we present contour plots of the vorticity, plots of the energy spectrum, the spectral decay in the vorticity, and plots of the norms of the large scale and small scale components of the solution, for the two methods considered.

In the test, we chose the forcing $f$ to be zero. The initial data $\omega_0$ for the vorticity was chosen so that the Fourier coefficients of the corresponding stream function $\psi_0$ satisfied:

$$|\psi_0(k_1, k_2)| = \left\{ \begin{array}{ll} C_1 \left\{ |\mathbf{k}|^{-2} [1 + (|\mathbf{k}|/6)^6] \right\}^{1/2}, & |\mathbf{k}| < 20.5 \\ 0, & |\mathbf{k}| \geq 20.5 \end{array} \right\}$$

as in Browining and Kreiss [2]. The phases of the Fourier coefficients were chosen randomly from $[0, 2\pi]$. As described in [2], if we chose $C_1$ so that $|\omega_0|_\infty = 1$, then we can approximately evaluate $|Du|_\infty$. For this particular choice of $C_1$, and for a kinematic viscosity $\nu = 5.0 \times 10^{-4}$, we obtain an estimate for the number of modes required to resolve the flow to be:

$$N_{max} \approx 34.$$

In the test, we therefore chose 64 modes in each direction, for the pseudo-spectral method, with:

$$\omega_{PS} = \sum_{|k_1| \leq 31} \sum_{|k_2| \leq 31} \hat{\omega}(k_1, k_2) e^{i(k_1 x + k_2 y)}.$$

For the non-linear Galerkin method, we chose 32 modes in each direction for the large scale component (extended by its small scale component so that there are still $64 \times 64$ modes in their sum). i.e.,

$$\omega_{NGM} = p + q,$$

where

$$p = \sum_{|k_1| \leq 15} \sum_{|k_2| \leq 15} \hat{p}(k_1, k_2) e^{i(k_1 x + k_2 y)},$$

and

$$q = \sum_{|k_1| \leq 15} \sum_{16 \leq |k_2| \leq 31} \hat{q}(k_1, k_2) e^{i(k_1 x + k_2 y)}$$

$$+ \sum_{16 \leq |k_1| \leq 31} \sum_{|k_2| \leq 15} \hat{q}(k_1, k_2) e^{i(k_1 x + k_2 y)} + \sum_{16 \leq |k_1| \leq 31} \sum_{16 \leq |k_2| \leq 31} \hat{q}(k_1, k_2) e^{i(k_1 x + k_2 y)}.$$

The total number of modes for $p+q$ is therefore $64 \times 64$.

For the above choice of initial data $\omega_0$, the energy $E(l)$ is proportional to $l^{-3}$ for large $l$, where $E(l)$ represents the energy corresponding to wavenumbers of magnitude $l$:

$$E(l) \equiv \frac{1}{2} \sum_{|\mathbf{k}| \in I_l} (|\hat{u}|^2 + |\hat{v}|^2) = \frac{1}{2} \sum_{|\mathbf{k}| \in I_l} |\mathbf{k}|^2 |\hat{\psi}|^2, \quad \text{for } I_l \equiv [l - 0.5, l + 0.5). \tag{7}$$

Similarly, a quantity $W(l)$ representing the average magnitude of the Fourier coefficients of $\omega_N$ of wavenumber $l$ is defined:

$$W(l) \equiv \left( \sum_{|\mathbf{k}| \in I_l} |\omega(\hat{\mathbf{k}})| \right) / \left( \sum_{|\mathbf{k}| \in I_l} 1 \right). \tag{8}$$

These quantities are computed in the numerical tests.

In Figure 1, we present the contour plots of the the vorticity, obtained by both the pseudo-spectral method, and the non-linear Galerkin method, at time $T \approx 5.0$. In Figure 2, the contour plots at time $T \approx 40.0$ is presented. The times are not exactly 40.0, since variable time steps were chosen by using the CFL condition. In Figure 3 we compare the energy spectrum of the solution at time $T \approx 5.0$ and $T \approx 40.0$ obtained by both methods. Figure 4 is a similar plot of the quantity $W(l)$ defined in (8), at times $T \approx 5.0$ and $T \approx 40.0$. In Figure 5 we plot the norms of the components $\|p\|$, $\|q\|$ and $\|q_t\|$ as functions of time, to see whether the approximation that $\|q\| \ll \|p\|$ and $\|q_t\| \ll \|p\|$ is accurate.

**A discussion on the numerical results.** The results in Figures 1 through 5 indicate that the non-linear Galerkin method based on $N/2$ modes (plus the remaining modes defining the small scale component $q$) gives solutions which are similar to those obtained by the pseudo-spectral method with $N$ modes. Since only half the number of modes were used for $p$ in equation (6), the non-linear Galerkin, can use times steps $\Delta t$ which are twice as large as that required by CFL limitations for the corresponding pseudo-spectral method with $N$ modes. However, the evaluation of $\Phi(p)$ as well as $B(p+\Phi(p))$ requires some 2D FFT's involving $N$ modes in each direction, rather than $N/2$ modes in each direction. Overall, there is a reduction in computational cost by a fixed fraction, due to the presence of the larger time step allowed in the non-linear Galerkin method.

Along another line, it was observed that if the number of modes $N/2$ used to represent the large scale solution $p$ was not sufficiently large, then the function $\Phi(p)$

Figure 1: Contour plots of the vorticity at $T \approx 5.0$

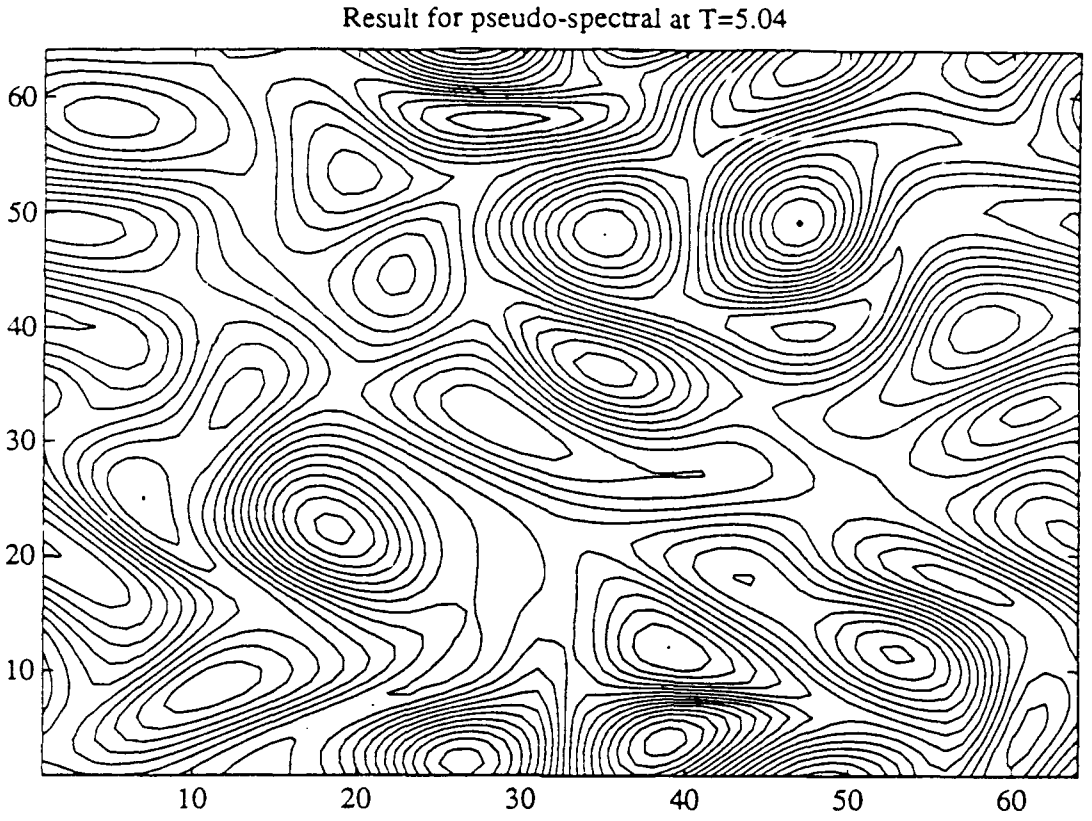


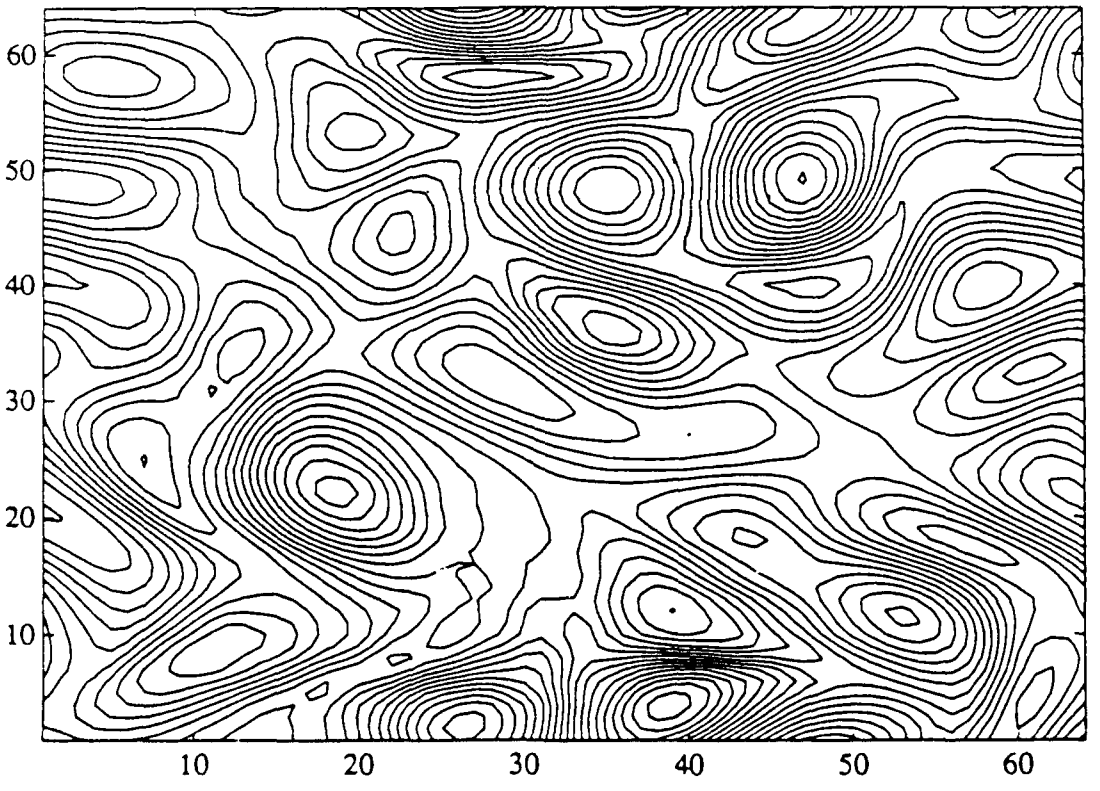

Figure 2: Contour plots of the vorticity at $T \approx 40.0$

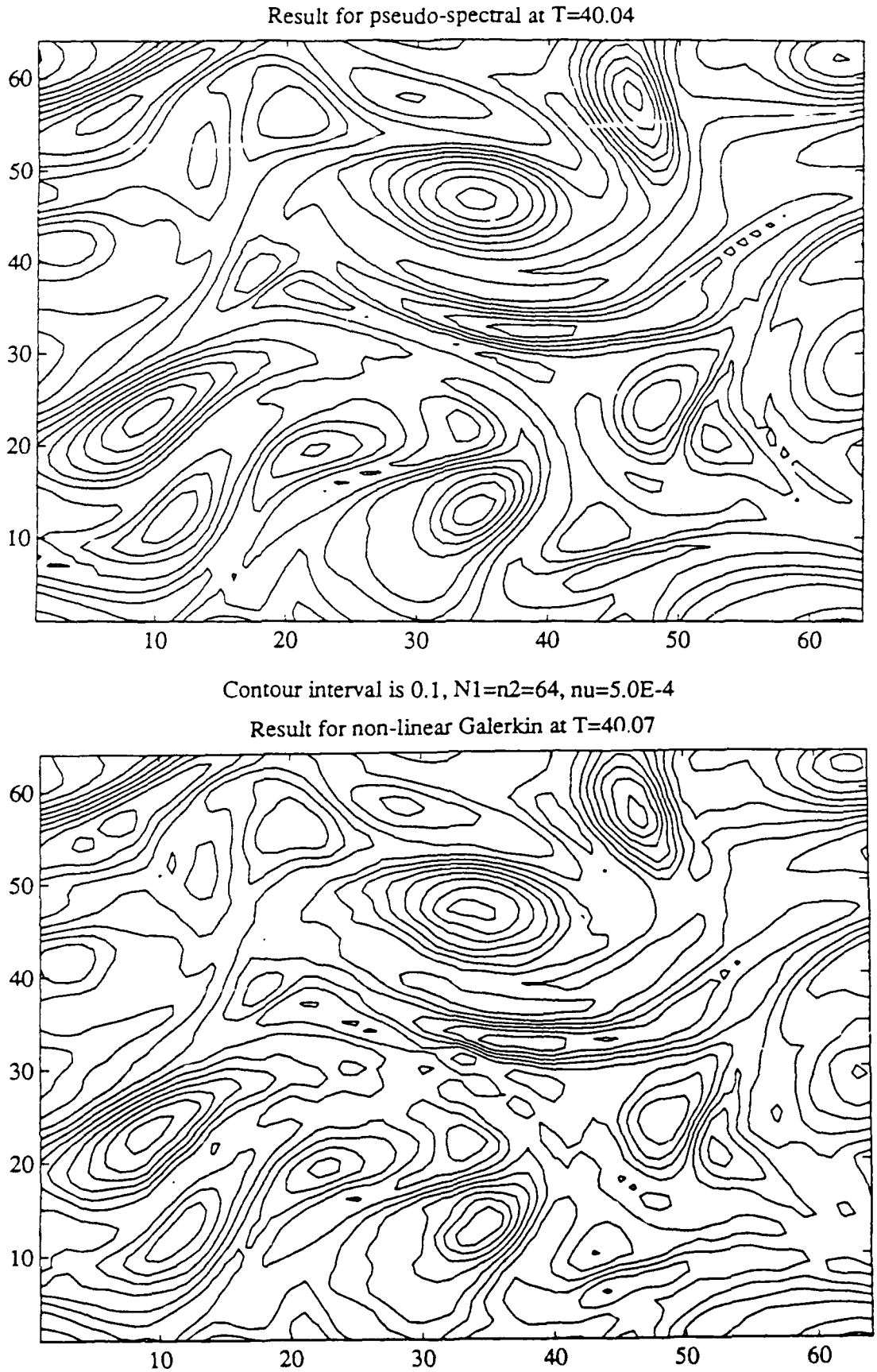

Figure 3: Energy spectrum $E(l)$

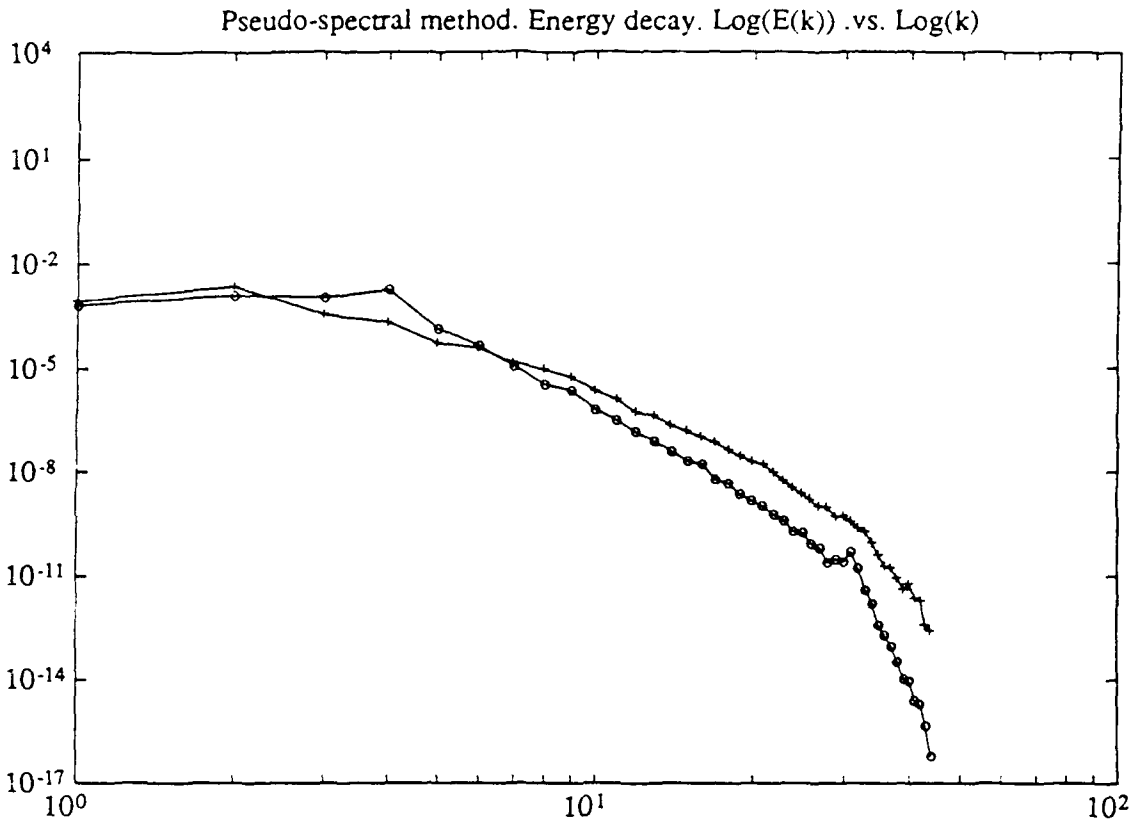


T=5.04 marked "o"; T=40.04 marked "+"; nu=5.0E-4; N=64

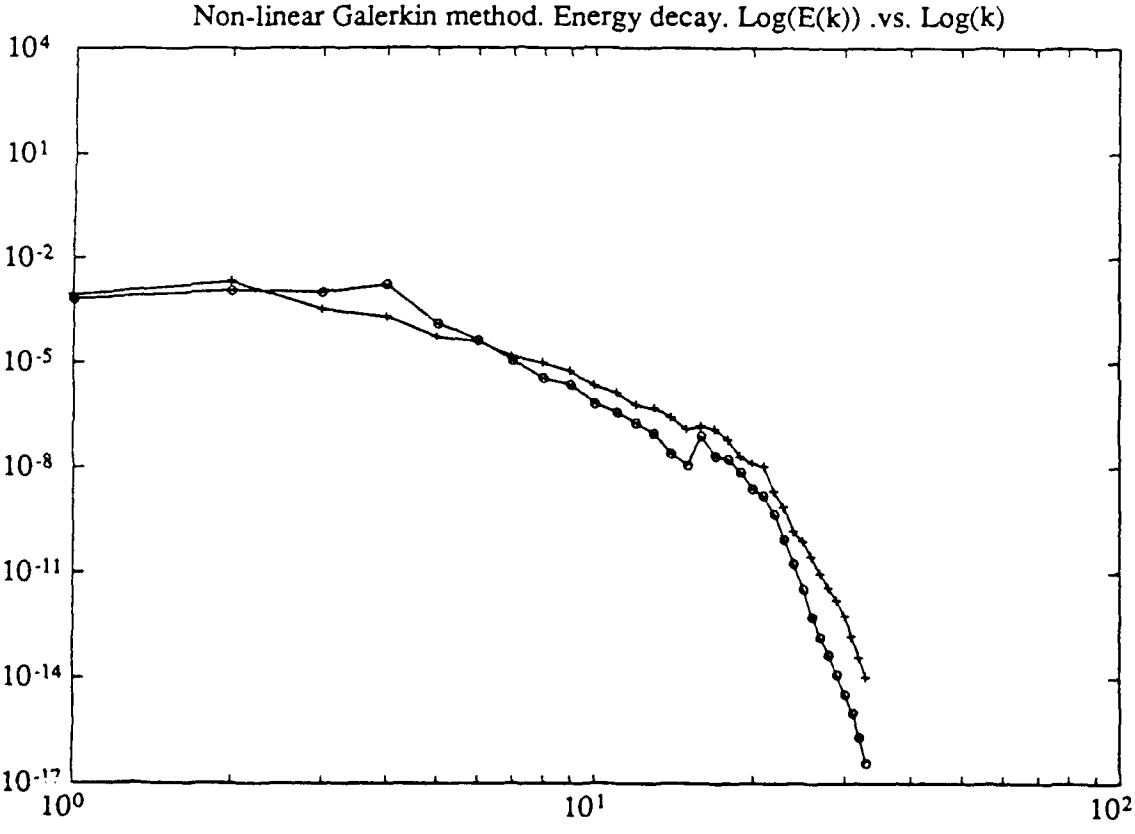


T=5.08 marked "o"; T=40.08 marked "+"; nu=5.0E-4; N=64; N/2=32

Figure 4: Spectral decay of vorticity

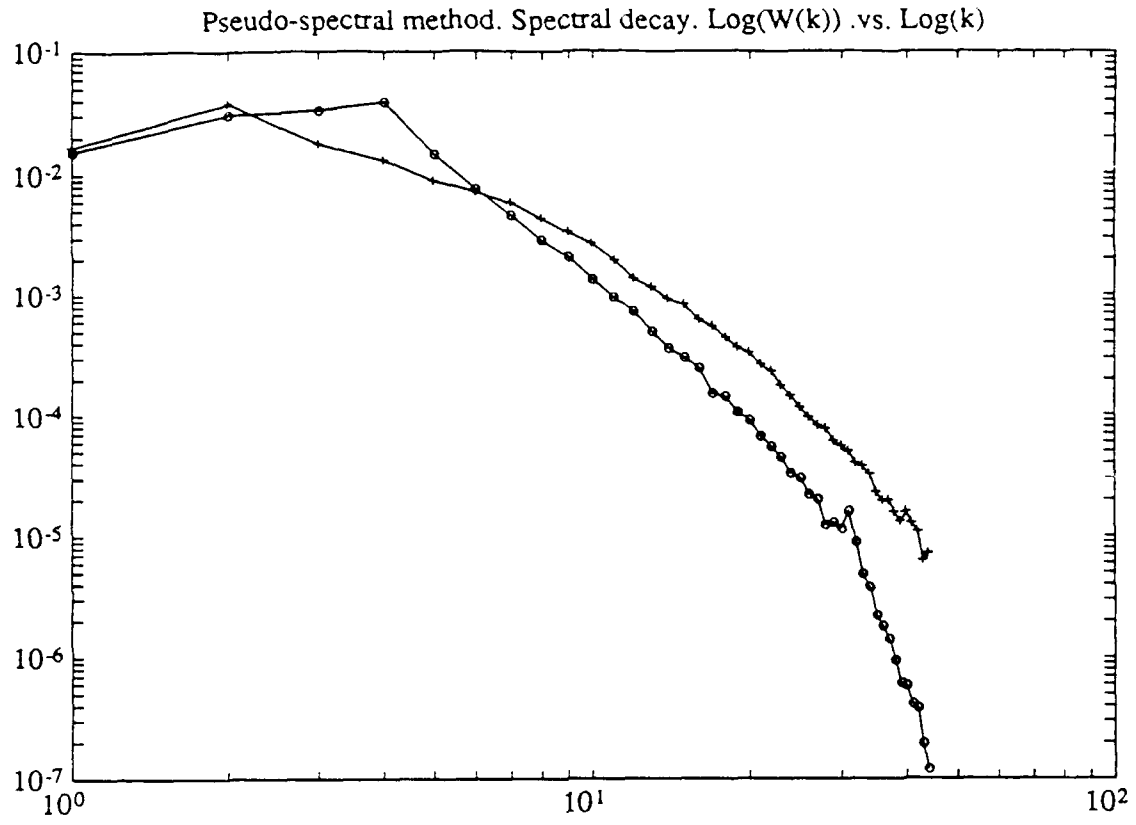


T=5.04 marked "o"; T=40.04 marked "+"; nu=5.0E-4; N1=N2=64

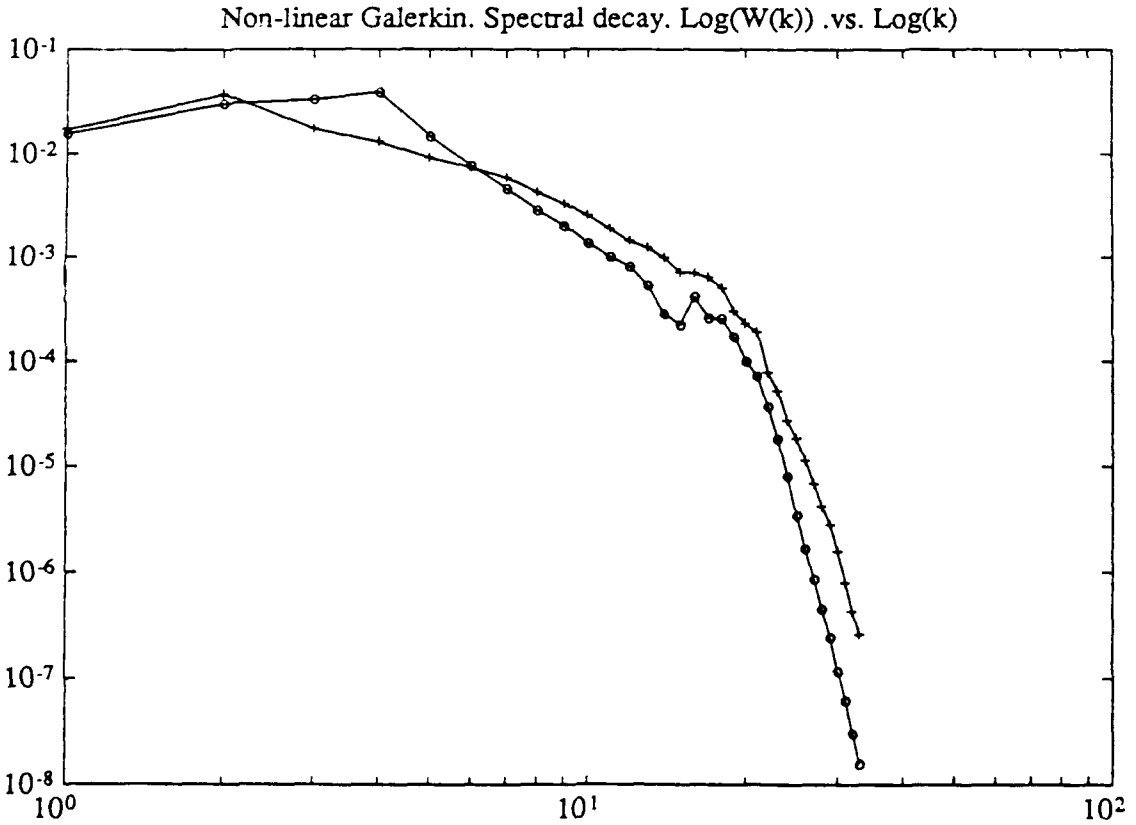


T=5.08 marked "o"; T=40.08 marked "+"; nu=5.0E-4; N=64, N/2=32

Figure 5: Norms of $\|p\|$, $\|q\|$ and $\|q_t\|$.

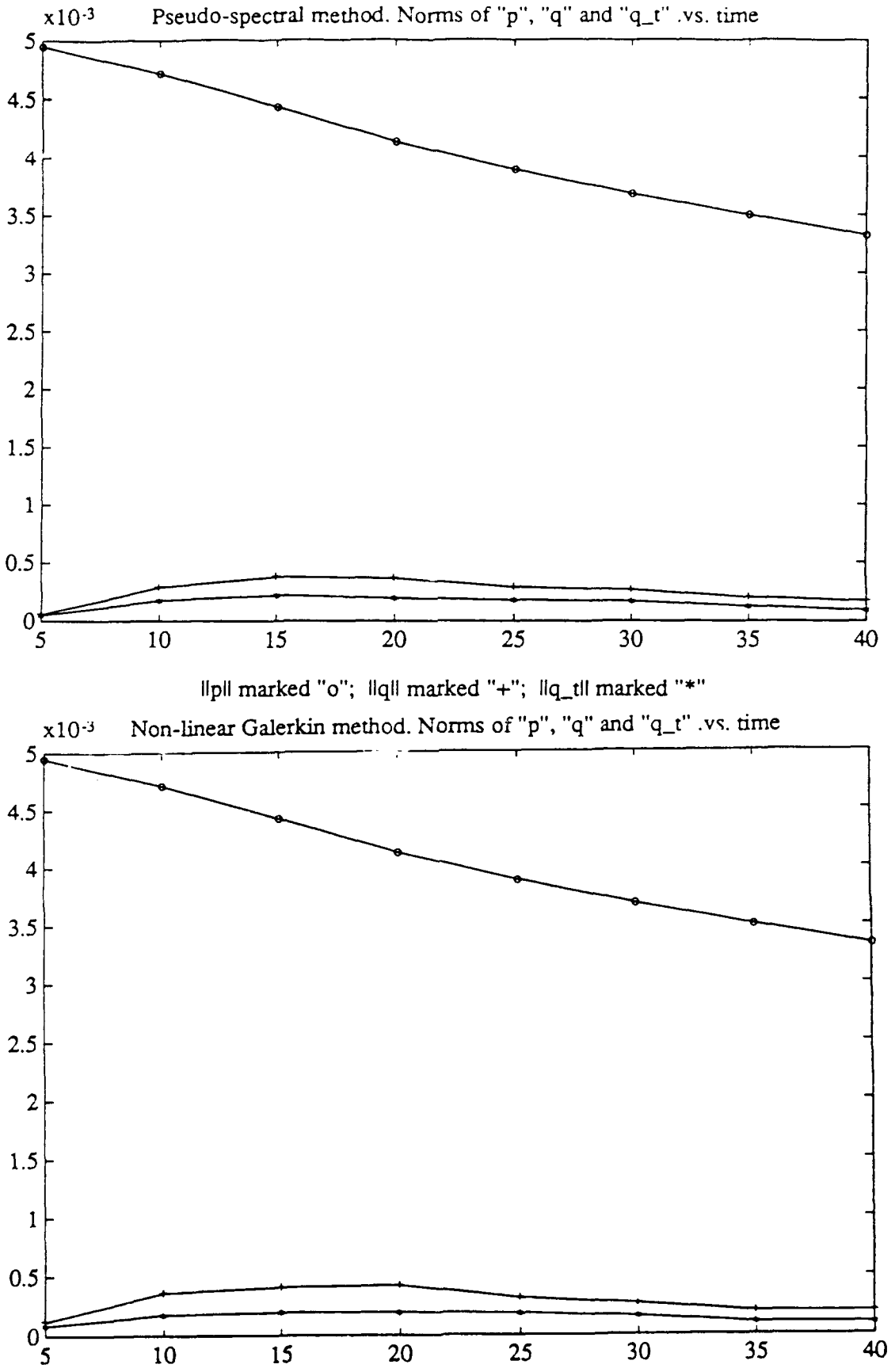

became large and an instability developed. We attribute this to the following. Since, by the definition of $\Phi(p)$:

$$\hat{q}(\mathbf{k}\ ) = \widehat{\Phi(p)}(\mathbf{k}) \equiv (\nu|\mathbf{k}|^2)^{-1}\left\{\hat{f}(\mathbf{k}) - \widehat{B(p)}(\mathbf{k})\right\}, \quad \text{for indices } |\mathbf{k}| \geq cN$$

it follows that if the divisor $\nu|\mathbf{k}|^2$ is small, then the corresponding Fourier modes are magnified, and an instability can result. This can be fixed by requiring the number of modes $N/2$ to be sufficiently large, so that:

$$\nu|\mathbf{k}|^2 \geq 1, \quad \text{for } |\mathbf{k}| \geq cN.$$

This requirement leads indirectly to a similar condition appearing in the minimum scale derived by Henshaw, Kreiss and Reyna [7]:

$$N \geq C\nu^{-1/2},$$

for some positive constant $C$.

We intend to perform more tests on these methods, including the case where the number of modes used is varied as the flow evolves into large scale structures, and also the use of hybrid algorithms. These may lead to accurate integrations over large time intervals with even more reduced computational cost.

# 6 Elliptic solvers

Finally, we briefly summarise results of related studies on efficient and easily parallelisable methods for solving elliptic problems [3], which can be applied to those linear systems which occur in time stepping the Navier-Stokes equations. Our studies have been based on two well known domain decomposition algorithms [1] [12]. They are based on a partition of the domain into many non-overlapping subregions, and a preconditioner is developed for the resulting reduced interface problem. The preconditioner essentially corresponds to a block Jacobi method, where the blocks correspond to couplings between unknowns on certain subregions of the interface. The subregions of the interface are chosen to be the edges separating the subdomains, a coarse grid consisting of the vertices of the subdomains, and cross-shaped regions centered about the vertices. Our studies have focused on replacing the exact blocks of the reduced interface matrix, by spectrally equivalent preconditioners, as this significantly reduces

the over head cost. Numerical experiments confirm theoretical results indicating that the resulting preconditioner has an optimal rate of convergence [3]. With the use of fast Poisson solvers on the subdomains, the resulting algorithm can be implemented in $O(N \log(N))$ operations where $N$ is the number of unknowns. Such algorithms can also be applied to indefinite linear systems, such as those obtained by discretisations of the velocity - pressure formulation of the Navier-Stokes equations [11].

# References


[1] J. H. Bramble, J. E. Pasciak and A. H. Schatz, *The construction of preconditioners for elliptic problems by substructuring, I*, Math. Comp., 47(175): 103-134, 1986.

[2] G. L. Browning and H.-O. Kreiss, *Comparison of numerical methods for the calculation of two-dimensional turbulence,* Mathematics of Computation, Vol. 52, No. 186, pages 369-388, April 1989.

[3] T. F. Chan and T. P. Mathew, *An application of the probing technique to the vertex space method in domain decomposition,* Tech. Report 90-22, UCLA, Department of Mathematics, Oct. 1990. Submitted to Proceedings of Domain Decomposition Conference held in Moscow.

[4] P. Constantin, C. Foias and R. Temam, *Attractors representing turbulent flows,* in Mem. Amer. Math. Soc. 53, No. 314, 1985.

[5] J. H. Ferziger, in *Computational methods for turbulent, transonic and viscous flows,* J. E. Essers (de.), Hemisphere Pub. Washington, 1983.

[6] J. H. Ferziger, in *Theoretical approaches to turbulence*, Dwoyer et al (eds.), Springer-Verlag, New York, 1985.

[7] W. D. Henshaw, H.-O. Kreiss and L. G. Reyna, *On the smallest scale for the incompressible Navier-Stokes equations*, CAM Report 88-10, UCLA, Department of Mathematics, March 1988.

[8] M. Marion and R. Temam, *Nonlinear Galerkin Methods,* SIAM J. Numer. Anal., Vol. 26, No. 5, pp. 1139-1157, October 1989.

[9] J. M. McDonough and R. J. Bywater, *Turbulent solutions from an unaveraged additive decomposition of Burgers' equation*, Forum on Turbulent Flows – 1989, Bower and Morris (eds.), ASME FED Vol. 76, New York, 1989.

[10] J. M. McDonough and R. J. Bywater, *Large scale-effects on local small-scale chaotic solutions to Burgers' equation*, AIAA Journal, Vol. 24, No. 12, pp. 1924-1930. December 1986.

[11] J. Pasciak, *Two Domain Decomposition Techniques for Stokes Problems,* In T. Chan, R. Glowinski, J. Periaux and O. Widlund, editors, Second International Symposium on Domain Decomposition Methods for Partial Differential Equations, Philadelphia, PA, 1988, SIAM.

[12] B. F. Smith, *An optimal domain decomposition preconditioner for the finite element solution of linear elasticity problems*, Technical Repot 482, Courant Institute, 1989. To appear in SIAM J. Sci. Stat. Comput.

[13] R. Temam, *The Nonlinear Galerkin Method in Computational Fluid Dynamics,* To appear.

[14] E. S. Titi *On approximate inertial manifolds to the Navier-Stokes equations,* in Journal of mathematical analysis and applications, Vol. 149, No. 2, July 1, 1990, Academic Press, New York.